Redox Biology 53 (2022) 102326

Contents lists available at ScienceDirect

Redox Biology

journal homepage: www.elsevier.com/locate/redox

Fatty acids derived from apoptotic chondrocytes fuel macrophages FAO through MSR1 for facilitating BMSCs osteogenic differentiation

Zi-Yang Zheng [a,b,1], Tao Jiang [a,b,1], Zhen-Fei Huang [a,b,1], Bo Chu [a,b,c], Jun Gu [c], Xuan Zhao [a,b], Hao Liu [a,b], Jin Fan [a,b], Li-Peng Yu [a,b], Shu-Heng Jiang [d], Qing Li [d], Li-Peng Hu [d], Fan-Qi Kong [e], Lai Zhang [f,g], Qi Chen [f,g], Jian Chen [a,b,****], Han-Wen Zhang [f,g,***], Guo-Yong Yin [a,b,**], Shu-Jie Zhao [a,b,*]

[a] Department of Orthopedics, The First Affiliated Hospital of Nanjing Medical University, Nanjing, Jiangsu, 210029, China
[b] Jiangsu Institute of Functional Reconstruction and Rehabilitation, Nanjing, Jiangsu, 210029, China
[c] Department of Orthopedics, Xishan People's Hospital of Wuxi City, Wuxi, Jiangsu, 21405, China
[d] State Key Laboratory of Oncogenes and Related Genes, Shanghai Cancer Institute, Ren Ji Hospital, School of Medicine, Shanghai Jiao Tong University, Shanghai, 200240, China
[e] Department of Orthopedic Surgery, Spine Center, Changzheng Hospital, Naval Medical University, Shanghai, 200003, China
[f] Department of Pathophysiology, Nanjing Medical University, Nanjing, 211166, China
[g] Key Laboratory of Jiangsu Province on Targeted Intervention of Cardiovascular Diseases, Nanjing, 211166, China

ARTICLE INFO

Keywords:
Macrophage
Fatty acid oxidation
MSR1
Apoptotic chondrocyte
Osteogenic differentiation

ABSTRACT

The nonunion following a fracture is associated with severe patient morbidity and economic consequences. Currently, accumulating studies are focusing on the importance of macrophages during fracture repair. However, details regarding the process by which macrophages facilitate endochondral ossification (EO) are largely unknown. In this study, we present evidence that apoptotic chondrocytes (ACs) are not inert corpses awaiting removal, but positively modulate the osteoinductive ability of macrophages. *In vivo* experiments revealed that fatty acid (FA) metabolic processes up-regulated following EO. *In vitro* studies further uncovered that FAs derived from ACs are taken up by macrophages mainly through macrophage scavenger receptor 1 (MSR1). Then, our functional experiments confirmed that these exogenous FAs subsequently activate peroxisome proliferator-activated receptor α (PPARα), which further facilitates lipid droplets generation and fatty acid oxidation (FAO). Mechanistically, elevated FAO is involved in up-regulating the osteoinductive effect by generating BMP7 and NAD^+/SIRT1/EZH2 axis epigenetically controls BMP7 expression in macrophages cultured with ACs culture medium. Our findings advanced the concept that ACs could promote bone regeneration by regulating metabolic and function reprogram in macrophages and identified macrophage MSR1 represents a valuable target for fracture treatments.

1. Introduction

The population suffering from fractures is increasing worldwide, and the failure of fracture repair with resulting nonunion is still a very challenging but devastating complication [1]. Despite intense clinical and research efforts, this problem has an estimated incidence of approximately 10% in all patients and leads to disability and a substantial economic burden [1]. In general, during fracture healing, new bone forms through intramembranous ossification (IO) and endochondral ossification (EO) [2]. IO is associated with the direct osteogenic

* Corresponding authors. Department of Orthopedics, The First Affiliated Hospital of Nanjing Medical University, Nanjing, Jiangsu, 210029, China. .
** Corresponding author. Department of Orthopedics, The First Affiliated Hospital of Nanjing Medical University, Nanjing, Jiangsu, 210029, China. .
*** Corresponding authors. Department of Pathophysiology, Nanjing Medical University, Nanjing, 211166, China. .
**** Corresponding author. Department of Orthopedics, The First Affiliated Hospital of Nanjing Medical University, Nanjing, Jiangsu, 210029, China. .
E-mail addresses: cbccj@sina.com (J. Chen), hanwenzhang@njmu.edu.cn (H.-W. Zhang), guoyong_yin@sina.com (G.-Y. Yin), zhaoshujie@njmu.edu.cn (S.-J. Zhao).
[1] These authors are co-first authors and contributed equally to this work.

https://doi.org/10.1016/j.redox.2022.102326
Received 1 March 2022; Received in revised form 18 April 2022; Accepted 27 April 2022
Available online 30 April 2022

differentiation of mesenchymal stem cells (MSCs) [2]. However, the classic EO model requires chondrocytes to mature toward hypertrophy, undergo apoptosis and eventually be replaced by new bone [2]. Recently, a critical role for macrophages in EO has been suggested [3]. Schlundt et al. revealed that fracture repair was delayed and callus mineralization was impaired in macrophage-depleted mice [3]. However, few details regarding the process by which macrophages facilitate EO are currently known.

The transition zone (TZ) represents a unique chondro-osseous junction that is composed mainly of hypertrophic apoptotic chondrocytes (ACs) and new osteoblasts during EO [3–5]. Notably, macrophages were also detected in this area [6]. Macrophages are highly dynamic, multifunctional cells that are activated in response to different microenvironmental stimuli [7]. To our knowledge, the functions and molecular mechanisms of macrophages in the TZ have not been revealed. A better understanding of the role of macrophages in this microenvironment is important for elucidating the process of fracture repair and might be helpful to develop novel therapeutic interventions that will improve clinical outcomes.

Traditionally, apoptosis is a fundamental biological process , and apoptotic cells are regarded as inert cells waiting for removal [8]. Remarkably, a recent study showed that apoptotic cells release specific metabolites to alter the expression of certain genes in adjacent normal cells [9]. As mentioned above, a large number of ACs and a group of macrophages are observed in the TZ. An interesting and important goal is to clarify the interplay between ACs and macrophages. Chondrocytes function by storing lipids in large quantities, and the intracellular lipid pattern might be altered by degeneration and apoptosis [10]. Researchers have not determined whether lipid-related metabolites from ACs induce specific gene programs in macrophages during fracture repair.

Macrophage scavenger receptor 1 (MSR1, also known as SR-A1 and CD204) belongs to the class A scavenger receptor family and orchestrates many functions in homeostasis [11]. However, the contribution of MSR1 to the macrophage phenotype and function does not appear to be black or white. For instance, MSR1 has recently been identified as a marker for tumor-associated macrophages (M2-like phenotype) that promote tumor progression and metastasis [12]. While, in interleukin 4 (IL-4)-activated macrophages, MSR1 promotes JNK activation and leads to a phenotypic switch from an M2-like to an M1-like state [13]. Thus, MSR1 has been proposed to induce both pro-M1-like and pro-M2-like properties, depending on the microenvironmental stimuli. In our previous study, MSR1 depletion in macrophages cocultured with bone marrow stem cells (BMSCs) inactivated M2-like polarization by affecting oxidative phosphorylation (OXPHOS) [14]. Moreover, a lack of MSR1 in macrophages decreases the osteogenic differentiation of MSCs during IO [14]. However, the specific function of MSR1 expressed in macrophages during EO and the molecular mechanisms remain unclear.

Here, we present evidence that fatty acid (FA) metabolic processes varied during EO on day 14 post fracture. Furthermore, FA uptake by MSR1 activated peroxisome proliferator-activated receptor α (PPARα), which further induced lipid droplet (LD) formation and fatty acid oxidation (FAO). Our study also elucidated that upregulated FAO subsequently activated the respiratory chain in macrophages to facilitate the osteogenic differentiation of BMSCs via nicotinamide adenine dinucleotide (NAD^+) generation. Mechanistically, due to the elevated level of NAD^+, decreased levels of acetylated EZH2 with methyltransferase activity mediated by the activation of the deacetylase Sirtuin1 (SIRT1) were observed. Moreover, we confirmed that the NAD^+/SIRT1/EZH2 axis effectively increased BMP7 expression in macrophages following exposure to ACs culture medium (CM). Altogether, our findings indicate a previously unrecognized effect of AC CM-mediated metabolic and functional reprogramming of macrophages and identify that MSR1 expressed in macrophages is the key protein contributing to this process, providing a potential target for fracture repair.

2. Results

2.1. FAs derived from ACs induce LD formation in macrophages

In a standardized mouse femoral fracture model, the growth of a cartilaginous callus driven by chondrocytes occurs approximately 7–10 days after fracture [15,16]. At approximately 10–14 days post fracture, chondrocytes gradually undergo apoptosis coupled with new bone formation, and we focused on a unique chondro-osseous junction defined as the TZ [15,16]. As shown in Fig. 1A and Sup Fig. 1A, compared with day 7, apoptosis of hypertrophic chondrocytes occurred at day 14 post fracture, and a large number of ACs were observed in the TZ. Consistent with previous reports, histological evidences further distinguished the chondro-osseous junction and revealed a group of macrophages localized within the TZ (Fig. 1A and Sup Fig. 1B and C) [3,17]. We analyzed three GEO datasets (GSE99118, GSE99580 and GSE15267) to provide an overall view of molecular events occurring on day 7 and day 14 during the EO fracture repair processes (Fig. 1B and Sup Fig. 1D–F). Interestingly, the bioinformatics analysis revealed that certain metabolism-related events, especially lipid and FA metabolic processes, were upregulated on day 14 post fracture among all three GEO datasets (Fig. 1B and Sup Fig. 1E). Therefore, we conducted a lipidomic analysis to directly probe lipid metabolic activity in the TZ during EO. As revealed in Fig. 1C and D and Sup Fig. 1G, several FA species were significantly enriched in the TZ of a callus on day 14 post fracture compared with day 7 post fracture.

As ACs could release certain metabolites that diffuse to affect surrounding cells, we wondered whether the elevated FAs present in the TZ on day 14 post fracture were derived from ACs. For further validation, we first optimized the parameters using chondrocytes, such that more than 90% of chondrocytes underwent apoptosis when treated with staurosporine (STS) (Fig. 1E). Next, targeted lipidomic analysis was performed on the culture medium (CM) from apoptotic and control chondrocytes. The heatmap and principal component analysis shown in Fig. 1F and G clearly certified that AC CM contained a large amount of FAs compared to the control group. Notably, 4 significantly upregulated FAs (C22:5, C22:4, C20:4 and C20:3) were shared between AC CM and the callus at day 14 post fracture, possibly due to differences and complexity in cell types and/or modality of death in the callus (Fig. 1H). We also prepared a FA mixture (FA mix) of these four long-chain FAs (LCFAs, C16–C22) to better investigate the role of crucial AC-derived FAs in regulating macrophage functions. Then, we tested whether neighboring macrophages were potentially influenced by ACs by incubating bone marrow-derived macrophages (BMDMs) with CM from apoptotic and normal chondrocytes (Fig. 1I). As shown in Fig. 1I, an obvious increase in LD formation was observed in BMDMs treated with AC CM using transmission electron microscopy (TEM). We semi-quantitatively analyzed the increased lipid levels in AC CM-treated BMDMs using the lipophilic fluorescent dye BODIPY 493/503. The flow cytometry results confirmed that both AC CM- and FA Mix-treated BMDMs exhibited significantly greater lipid accumulation than the corresponding control cells (Fig. 1J and K). Moreover, we isolated $CD45^+CD11b^+F4/80^+$ macrophages within the area of the TZ on day 7 and day 14 post fracture to confirm the potential associations identified above (Fig. 1L and Sup Fig. 1G). Compared to macrophages collected from the TZ on day 7 post fracture (the stage of chondrocyte proliferation), callus-sorted macrophages from the TZ on day 14 post fracture (the stage of chondrocyte apoptosis) displayed significantly increased neutral lipid contents (Fig. 1M and N). Collectively, these results clearly showed that FAs released from ACs induce lipid accumulation in macrophages.

2.2. Macrophages accumulate lipids through increased FA uptake via MSR1

Specific inhibitors to block critical steps in de novo synthesis

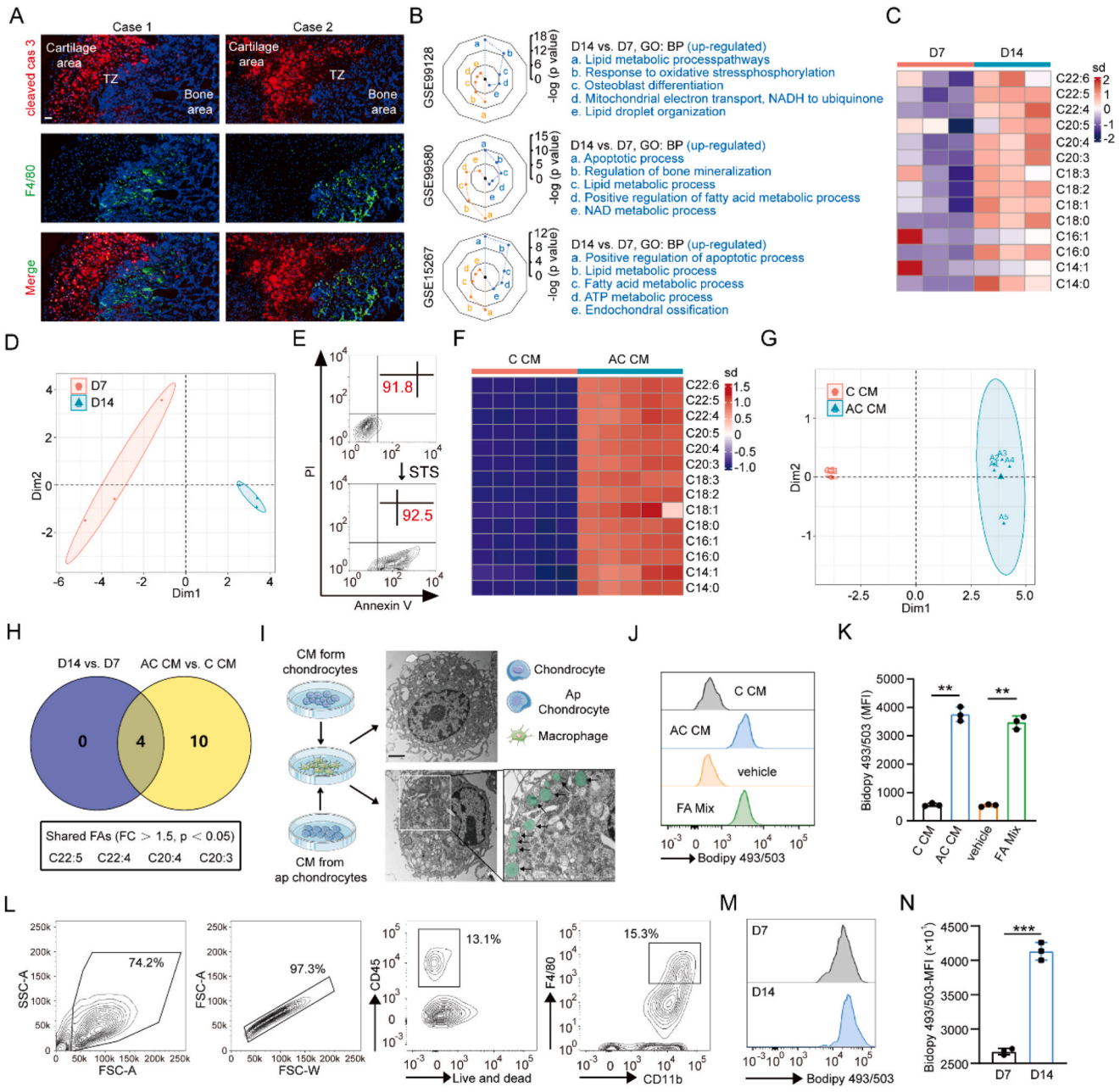

Fig. 1. Apoptotic chondrocytes (ACs) induce lipid droplet (LD) formation in macrophages by releasing fatty acids (FAs).
(A) The distribution of ACs and macrophages in the transition zone (TZ) from the callus on day 14 (D14) post fracture was assessed. Representative images of IF staining for cleaved caspase3 (red) and F4/80 (green) are shown, and the cell nuclei were stained with DAPI (blue). Scale bars, 100 μm. (B) Lipid and FA metabolic processes were upregulated on day 14 (D14) post fracture, according to the bioinformatics analysis. Representative biological process (BP) categories obtained from GO analyses of upregulated differentially expressed genes (DEGs) and downregulated DEGs (Sup Fig. 1F) between two time points (D14 vs. D7) after bone fracture in three different GEO datasets (GSE99118, GSE99580 and GSE15267). (C) Heatmap produced from the lipidomic analysis of callus tissues in the TZ on D14 relative to D7 post fracture (n = 3). sd, standard deviation. (D) Principal component analysis (PCA) of lipidomic data from callus tissues in the TZ on D14 and D7 post fracture with three biological replicates. (E) ACs induced by staurosporine (STS) were analyzed using flow cytometry after staining with FITC-Annexin V and propidium iodide. More than 90% of chondrocytes were apoptotic in the STS-treated group. (F) Heatmap from the lipidomic analysis of culture medium (CM) representing the FAs that were statistically enriched in AC CM compared to the control group (n = 5). sd, standard deviation. (G) PCA of lipidomic data from AC CM and C CM (n = 5). (H) Venn diagrams depicting the 4 shared FAs (C22:5, C22:4, C20:4 and C20:3) in two lists (List 1: D14 vs. D7, List 2: AC CM vs. C CM). (I) Schematic of the experimental protocol for macrophages treated with AC CM or C CM. After stimulation with AC CM or C CM, the LDs in different groups were evaluated using transmission electron microscopy (TEM). Black arrows indicate LDs (green). Scale bars, 2 μm. (J and K) Flow cytometry analysis of lipid levels in BMDMs treated with AC CM or C CM and FA mix or vehicle controls. Representative histogram showing the levels of lipids in BMDMs in these groups (J). Statistical analysis of the mean fluorescence intensity (MFI) of lipids in BMDMs from the indicated groups (n = 3) (K). The results are presented as means ± s.d., **P < 0.001. (L) Gating strategy for sorting $CD45^+CD11b^+F4/80^+$ macrophages around the area of the TZ post fracture. (M and N) Intracellular lipid levels in macrophages from the TZ were analyzed on D7 and D14 post fracture. Representative histogram displaying the lipid levels in callus-sorted macrophages on D7 and D14 post fracture (M). Measurements of the MFI of lipids were performed in triplicate. Means ± s.d., ***P < 0.0001. (For interpretation of the references to color in this figure legend, the reader is referred to the Web version of this article.)

pathways were first used to investigate whether exogenous FAs or endogenous synthesized FAs account for AC CM-induced LD accumulation in macrophages (Sup Fig. 2A). As revealed in Fig. 2A and B and Sup Fig. 2A and B, neither the ACC (acetyl-coenzyme A [CoA] carboxylase) inhibitor 5-tetradecyloxy-2-furoic acid (TOFA) nor the FA synthase (FASN) inhibitor C75 decreased the elevated lipid levels stimulated by AC CM, suggesting that endogenous FAs are dispensable for AC CM-induced lipid accumulation. Furthermore, we observed that triacsin C (an inhibitor of long-chain acyl-CoA synthetase [ACSL]) almost completely inhibited lipid accumulation in BMDMs. Thus, ACSL might catalyze acyl-CoA production from FAs derived from AC CM during triglyceride synthesis (Fig. 2A and B, and Sup Fig. 2B). We took advantage of a lipid uptake assay using BODIPY 558/568C12 (Red C12) to directly evaluate FA uptake. In this assay, chondrocytes labeled with Red C12 underwent apoptosis following exposure to STS, and then the BMDMs were cultured with AC CM containing Red C12 (Fig. 2C). BMDMs took up Red C12 from AC CM, and these red fluorescently labeled FAs were subsequently incorporated into 493/503-positive LDs (Fig. 2D and Sup Fig. 2C). Notably, the amount of FA transfer from ACs to macrophages was significantly higher than that from ACs to chondrocytes, BMSCs, osteoblasts and osteoclasts, showing preferential transfer (Fig. 2D and Sup Fig. 2C). During the analyses described above, we found that FA uptake might be the main cause of lipid accumulation in macrophages.

Furthermore, we explored the key factors involved in FA uptake in BMDMs using high-throughput RNA sequencing (RNA-seq), including three biological replicates of C CM-treated BMDMs and AC CM-treated BMDMs (Fig. 2E and Sup Fig. 2D and E). Compared with their control counterparts, AC CM-treated BMDMs exhibited increased FA binding and transfer activities and scavenger receptor activity (Fig. 2F). Scavenger receptors are reported to play important roles in intracellular lipid transport [18]. However, their expression in macrophages after treatment with AC CM is still largely unknown. Thus, we tested the expression pattern of four major scavenger receptors: MSR1, CD36, CD68 and macrophage receptor with collagenous structure (MARCO). The results of RNA-seq and RT–qPCR indicated that AC CM significantly upregulated the *msr1* mRNA expression level in BMDMs (Fig. 2G and Sup Fig. 2F). Treatment with the FA mix also induced elevated *msr1* mRNA expression (Fig. 2G). Moreover, flow cytometry assays suggested that this change was associated with increased expression of the receptor on the surface of BMDMs (Fig. 2H). Additionally, macrophages collected from the callus within TZ on day 14 post fracture exhibited significantly higher MSR1 mRNA and protein expression than the control group (Fig. 2I and Sup Fig. 2G). We detected LD formation in MSR1 WT and KO BMDMs treated with AC CM and FA Mix and the respective controls to further validate the effect of MSR1 on FA uptake in macrophages. As shown in Fig. 2J-L and Sup Fig. 2H, MSR1-depleted BMDMs exhibited a significant decrease in lipid accumulation after culture with AC CM or FA Mix. We also obtained similar findings that MSR1 knockout in AC CM-treated BMDMs reduced the increased number of Red C12-positive 493/503 LDs (Fig. 2M and N). However, these effects were diminished in the C CM- and vehicle-treated MSR1 WT and KO BMDMs (Fig. 2J-N). We also noted that callus-sorted macrophages harvested from MSR1 KO mice on day 14 post fracture showed a lower LD content than those from the MSR1 WT mice (Fig. 2P and Sup Fig. 2J). In contrast, MSR1 depletion did not affect lipid accumulation in callus-sorted macrophages on day 7 post fracture (Fig. 2O and Sup Fig. 2I). Taken together, the upregulation of MSR1 plays a key role in FA uptake and LD formation in macrophages *in vivo* and *in vitro*.

2.3. Accumulated lipids are used to fuel FAO in macrophages treated with AC CM

Next, we asked whether lipid accumulation in macrophages has functional consequences. By comparing biological processes (BPs) induced in BMDMs by supernatants from ACs and control chondrocytes, we identified that lipid and FA metabolic processes were enhanced in AC CM-cultured BMDMs (Fig. 3A). We first measured the extracellular acidification rate (ECAR) (reflecting the activity of glycolysis) and mitochondrial oxygen consumption rates (OCR) (reflecting the activity of OXPHOS) using a Seahorse extracellular flux analysis in BMDMs treated with AC CM and C CM to test whether macrophages use the accumulated lipids as a fuel to produce energy (Fig. 3B and C and Sup Fig. 3A and B). Reduced glycolysis and glycolytic capacity and increased OCR, basal respiration, ATP production, respiratory capacity, and respiratory reserve were observed in AC CM-treated BMDMs (Fig. 3B and C and Sup Fig. 3A and B). The detection of lactate production also supported the finding that the AC CM treatment decreased the level of glycolysis (Fig. 3D). Next, we assessed FAO, by measuring the OCR after treatment with ETO (a FAO inhibitor), and the ΔOCR of basal respiration and respiratory capacity were calculated to assess the contribution of FAO to OXPHOS (Fig. 3C and E). The FAO capacity measured in BMDMs further highlighted that AC CM treatment facilitated FAO activity (Fig. 3C and E). Second, we tested the effect of FA-mediated metabolic reprogramming in macrophages using FA mix to verify this conclusion. As revealed in Sup Fig. 3C and D, the ECAR measurement suggested that FA mix decreased glycolysis. Compared to controls, the OCR and FAO were increased in FA mix-treated BMDMs (Sup Fig. 3*E*–G). Furthermore, we determined how macrophages use accumulated LDs as the energy source to fuel FAO. According to recent findings, LDs and mitochondrion form a functional organelle pair, facilitating FA transport from LDs to mitochondrion, where they are oxidized as an energy source to produce ATP [19]. Indeed, contact between these two organelles was observed in AC CM-treated macrophages using TEM (Fig. 3F). Secondary validation via IF staining indicated that the percentage of LDs interacting with mitochondrion was much higher in AC CM- and FA Mix-treated macrophages than in the control groups (Fig. 3G and Sup Fig. 3H). As an important metabolic pathway, FAO plays a complex role in shaping macrophage function and has attracted increasing attention in recent years [20]. The importance of FAO in regulating macrophage polarization status, particularly during fracture repair, has yet to be elucidated. As shown in Sup Fig. 3I and J, compared to control groups, macrophages treated with AC CM or FA mix were remarkably polarized to the M2-like phenotype. Finally, we tested the role of macrophage-derived MSR1 in managing cellular energy homeostasis in response to AC CM. Because MSR1 directly determines the level of FA uptake, we speculate that it is involved in FAO in macrophages. In response to AC CM, increased ECAR and lactate production were observed in BMDMs generated from MSR1 KO mice compared to WT BMDMs (Fig. 3H and I and Sup Fig. 3K). We also detected decreased OCR values, basal respiration, ATP production, respiratory capacity, and respiratory reserve in MSR1 KO BMDMs after treatment with AC CM (Fig. 3J-L). As expected, FAO and LD-mitochondrion contact were significantly attenuated in MSR1 KO BMDMs compared with WT BMDMs in response to AC CM (Fig. 3J and M). However, due to the lack of exogenous FAs, no significant difference was observed in the metabolic program (glycolysis, FAO and OXPHOS), and LD-mitochondrion interactions were not detected in MSR1 WT and KO BMDMs after culture with vehicle controls (Fig. 3H-M and Sup Fig. 3K and L). These data support the hypothesis that FA uptake by MSR1 promotes FAO and OXPHOS in macrophages to generate more energy.

2.4. PPARα activation by AC CM triggers LD generation and FAO in macrophages

A KEGG pathway analysis of differentially expressed genes (DEGs) between AC CM-treated BMDMs and C CM-treated BMDMs was performed to further identify the molecular mechanisms by which FA uptake by MSR1 triggers LD formation and subsequent FAO in macrophages. As indicated in Fig. 4A, the PPAR signaling pathway was significantly upregulated in BMDMs cultured with AC CM. PPARs are ligand-activated transcription factors (TFs) that play central roles in

lipid metabolism [21,22]. The data from the transcriptional analysis and RT–qPCR revealed that AC CM treatment upregulated the expression of ppara, but not pparb or pparg (Sup Fig. 4A and B). Additionally, studies have shown that fluctuating intracellular concentrations of FAs might alter PPARα activity. Therefore, we first examined the effects of AC CM treatment on PPARα activation by measuring nuclear PPARα levels. Compared with AC CM-treated MSR1 KO BMDMs, nuclear PPARα activity was markedly increased in AC CM-treated MSR1 WT BMDMs (Fig. 4B). The interpretation of this result is that MSR1 knockout reduces FA uptake by macrophages in response to AC CM. However, because of the lack of exogenous FAs, PPARα activities in MSR1 WT and KO BMDMs treated with C CM were similar, and both were significantly lower than those observed in cells treated with AC CM. We next tested the effect of FAs on nuclear PPARα activity in macrophages using FA Mix. A similar effect on macrophages was observed in response to FA Mix and vehicle controls (Sup Fig. 4C). We further confirmed that MSR1-mediated FA uptake is involved in PPARα activation by applying a small-molecule inhibitor targeting PPARα (GW6471). As displayed in Fig. 4C, compared to the MSR1 KO group, the protein levels of nuclear PPARα and CPT1A (a target gene for PPARα) were increased in MSR1 WT BMDMs treated with AC CM, while GW6471 decreased the levels of the nuclear PPARα and CPT1A proteins. In contrast, due to the lack of exogenous FAs, no difference in the expression patterns of nuclear PPARα and CPT1A were observed between MSR1 WT and KO BMDMs treated with or without GW6471 in the C CM group (Sup Fig. 4D). PPARα promotes LD formation by catalyzing acyl-CoA production from FAs and enhances FAO by transporting FAs into mitochondrion [23]. We subsequently examined the importance of PPARα in LD generation in

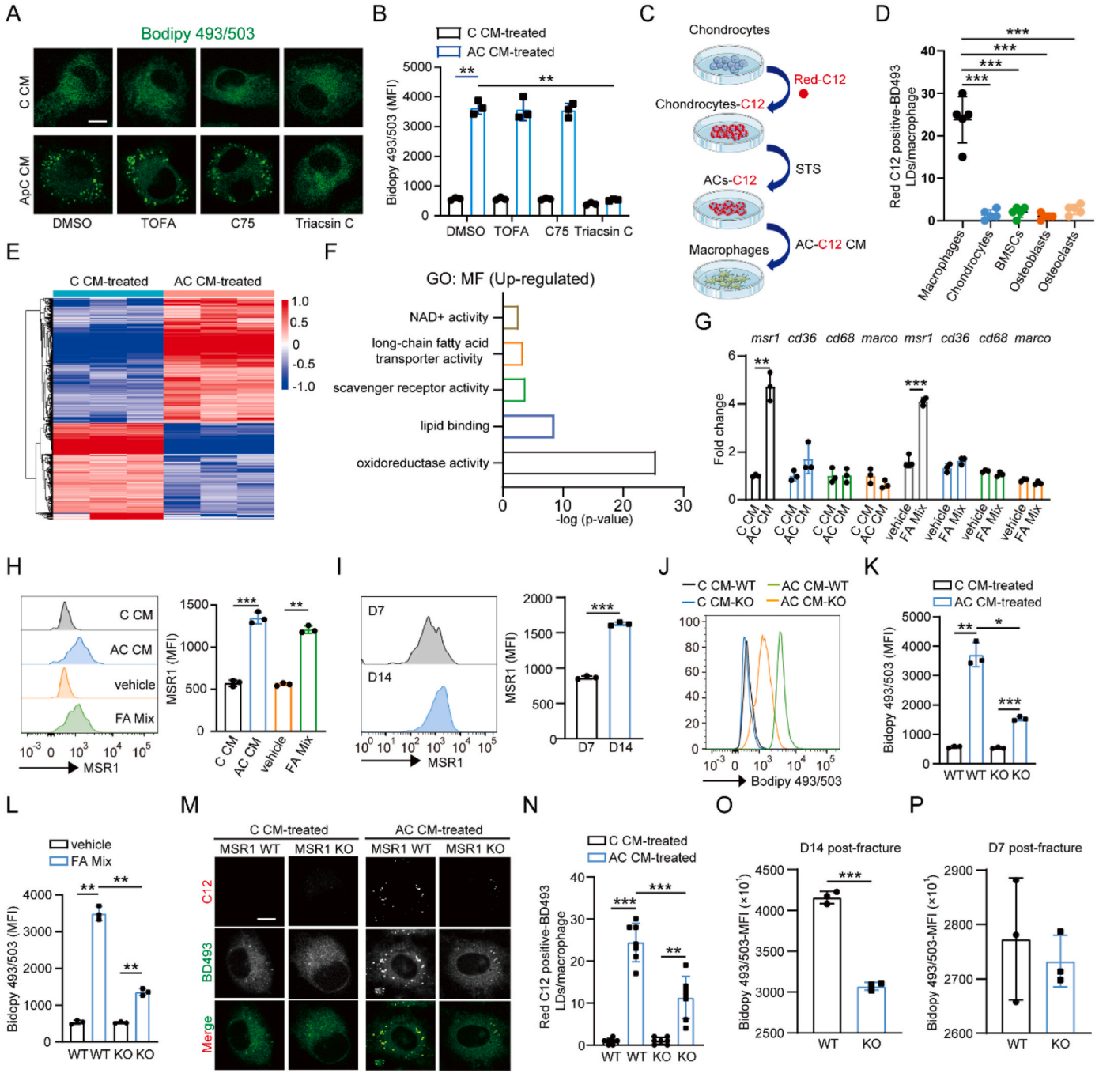

(caption on next page)

Fig. 2. MSR1 is essential for lipid accumulation in macrophages.
(A and B) Intracellular LDs in BMDMs cultured with AC CM or C CM in the presence of DMSO, TOFA, C75 and triacsin C were visualized using BODIPY 493/503 (A). Quantification of the MFI of intracellular lipids in BMDMs from the indicated groups (n = 3) (B). The results are presented as means ± s.d., **P < 0.001. Scale bars, 10 μm. (C) Schematic representation of the Red C12 transfer assay: chondrocytes were first incubated with Red C12, apoptosis was induced by STS, and then cells were washed and cultured with CM. Finally, C12-labeled CM was collected and used to treat macrophages to determine the uptake of FAs. (D) Quantification of Red C12-positive LDs following transfer between different cell types (n = 5). The results are presented as means ± s.d., ***P < 0.0001. (E) Heatmap of DEGs in AC CM-treated BDMDs compared to C CM-treated BMDMs. Blue and red colors represent low and high expression values, respectively. (F) Representative molecular function (MF) categories identified in GO analyses based on upregulated DEGs in AC CM-treated BDMDs compared to C CM-treated BMDMs. (G) Expression patterns of the indicated scavenger receptors in BMDMs treated with AC CM, C CM, vehicle and FA mix were determined using RT–qPCR. The results of three experiments are shown. Values are presented as means ± s.d., **P < 0.001, ***P < 0.0001. (H) Representative histograms (left panel) and statistical results (right panel) showing the expression of the MSR1 protein on the surface of BMDMs treated with AC CM, C CM, vehicle and FA mix (n = 3). Values are presented as means ± s.d., **P < 0.001, ***P < 0.0001. (I) Representative histograms (left panel) and statistical analysis of the MFI (right panel) show the expression of MSR1 on the surface of callus-sorted macrophages from the TZ on D7 and D14 post fracture (n = 3). Values are presented as means ± s.d., ***P < 0.0001 (J and K) Representative histograms (J) and statistical analysis of the MFI of BODIPY 493/503 (K) showing the effect of MSR1 on FA uptake in macrophages cultured with AC CM or C CM (n = 3). Values are presented as means ± s.d., ***P < 0.0001. (L) Results of the statistical analysis showing the lipid levels in WT and MSR1 KO BMDMs in response to treatment with FA mix or vehicle controls (n = 3). Values are presented as means ± s.d., **P < 0.001. (M and N) Loss of MSR1 in AC CM-treated BMDMs significantly attenuated FA uptake. Representative confocal images of WT and MSR1 KO BMDMs following the indicated transfer assays (M). Quantification of Red C12-positive LDs in WT and MSR1 KO BMDMs treated with AC CM or C CM following transfer assays (n = 8) (N). Values are presented as means ± s.d., ***P < 0.0001. Scale bars, 10 μm. (O and P) Knockout of MSR1 reduced the LD content in callus-sorted macrophages from the TZ on D14 but not on D7 post fracture. Results from the statistical analysis of the lipid levels in WT and MSR1 KO macrophages from the TZ on D14 (O) and D7 (P) post fracture are shown (n = 3). Values are presented as means ± s.d., ***P < 0.0001.

macrophages treated with AC CM by quantifying the fluorescence intensity of BODIPY 493/503 using flow cytometry. As indicated in Fig. 4D and E, GW6471 significantly decreased lipid accumulation in MSR1 WT and KO BMDMs treated with AC CM. We next hypothesized that activated PPARα is also required for facilitating FAO in macrophages cultured with AC CM. As expected, we found that PPARα activation triggered by FAs derived from AC CM plays an essential role in metabolic reprogramming by measuring lactate secretion, ECAR, OCR and FAO in MSR1 WT and KO BMDMs cultured in the presence or absence of GW6471 (Fig. 4F–I and Sup Fig. 4E and F). GW6471 treatment of MSR1 WT and KO BMDMs significantly increased the activities of glycolysis and lactate production (Fig. 4F and G and Sup Fig. 4E). In addition, inhibition of PPARα using GW6471 decreased FAO and OXPHOS in both MSR1 WT and KO BMDMs after culture with AC CM, as evidenced by the decreased values of FAO and OCR (Fig. 4H and I and Sup Fig. 4F). Moreover, the attenuated FAO and OXPHOS might also be partially attributed to the loss of contact between LDs and mitochondrion in GW6471-treated BMDMs treated with AC CM (Fig. 4J). These results clearly indicated that PPARα is activated in macrophages following MSR1-mediated FA uptake induced by treatment with AC CM, and activated PPARα is crucial for LD formation and FAO.

2.5. FAO in macrophages is required for the osteogenic differentiation of BMSCs after treatment with AC CM

According to the published literature, metabolites released from apoptotic cells are capable of regulating the tissue repair ability of neighboring cells [9]. We next asked whether the pro-osteogenic differentiation properties of macrophages were modulated by AC CM. Therefore, BMSCs were cultured with osteoblast differentiation medium in the presence or absence of CM from BMDMs treated with AC CM. Then, osteogenic differentiation was assessed using alizarin red (AR) staining and an ALP enzyme assay on day 7 and day 14. As shown in Fig. 5A and B, compared with the control group, a more pro-osteogenic differentiation effect was detected in BMSCs after culture with osteoblast differentiation medium and CM from AC CM-treated BMDMs. In addition, unlike the effect of AC CM, C CM did not alter the osteogenic differentiation of BMSCs *in vitro* (Sup Fig. 5A and B). The data in Sup Fig. 5C and D further illustrate the importance of FAs in regulating the pro-osteogenic differentiation properties of macrophages. Second, we attempted to investigate whether FAO in macrophages affects this increased osteoinductive effect. As indicated in Fig. 5A and B, the enhanced osteoinductive effect was significantly limited in BMSCs cultured with osteoblast differentiation medium and CM from CM-treated MSR1 KO BMDMs. Furthermore, after treatment with GW6471 (an inhibitor of PPARα) or ETO (an inhibitor of CPT1A), the enhanced osteoinductive effect was almost completely blocked (Fig. 5A and B). These results were also confirmed by quantifying the mRNA expression levels of osteogenic marker genes (collagen type I [*col1*], alkaline phosphatase [*alp*], osteocalcin [*ocn*], and runt-related transcription factor 2 [*runx2*]) in BMSCs from the indicated groups on day 7 and day 14 (Fig. 5C and D).

As MSR1-dependent exogenous FA uptaken by macrophages directly regulates PPARα activity, and activated PPARα subsequently induces LD formation and enhances FAO, we generated a femoral fracture model using MSR1 WT and KO mice to address the importance of MSR1 during EO *in vivo*. By comparing MSR1 KO and WT mice, 3D reconstruction images and analyses of morphometric parameters (callus volume/tissue volume [CV/TV]) clearly indicated that a lack of MSR1 significantly impaired EO (Fig. 5E and F). Quantification of callus bridging via X-ray images also suggested that MSR1 KO mice had lower union rates than MSR1 WT mice (Fig. 5G and Sup Fig. 5E). Therefore, these data indicate that elevated FAO might support the pro-osteogenic differentiation properties of macrophages in response to AC CM.

2.6. FAO-induced BMP7 production is necessary to positively regulate the osteogenesis of BMSCs in AC CM-treated macrophages

We first analyzed the RNA-seq data to explore which cytokines produced by macrophages upon exposure to AC CM facilitate the osteogenic differentiation of BMSCs. As shown in Sup Fig. 5F, the expression of three bone morphogenetic protein (BMP) family genes (*bmp3*, *bmp7*, and *bmp10*) was significantly increased in BMDMs cultured with AC CM versus C CM. Further verification using RT–qPCR revealed the mRNA expression pattern of *bmp* family genes in BMDMs in response to AC CM compared with C CM and FA mix versus the vehicle control (Sup Fig. 5G and H). As indicated in Fig. 6A, *bmp7* was the only shared gene in the three lists. Because metabolic rewiring modulates the functions of macrophages, we hypothesized that elevated FAO might increase BMP7 production. As shown in Fig. 6B and Sup Fig. 5I, the increased BMP7 mRNA and protein levels were significantly decreased in MSR1 KO BMDMs after culture with AC CM. Furthermore, the use of GW6471 targeting PPARα and ETO targeting CTP1A, but not 2-DG (glycolysis inhibitor), substantially reduced the elevated BMP7 level (Fig. 6B and C and Sup Fig. 5I and J). This correlation also supports our hypothesis that an increase in FAO is involved in the increased BMP7 production in WT BMDMs (Fig. 6D and Sup Fig. 5K). Next, we verified whether the positive effect of AC CM-treated BMDMs on the osteogenesis of BMSCs was due to increased BMP7 production. As revealed in Fig. 6E and F, the enhanced osteoinductive effect of CM from AC CM-treated BMDMs was

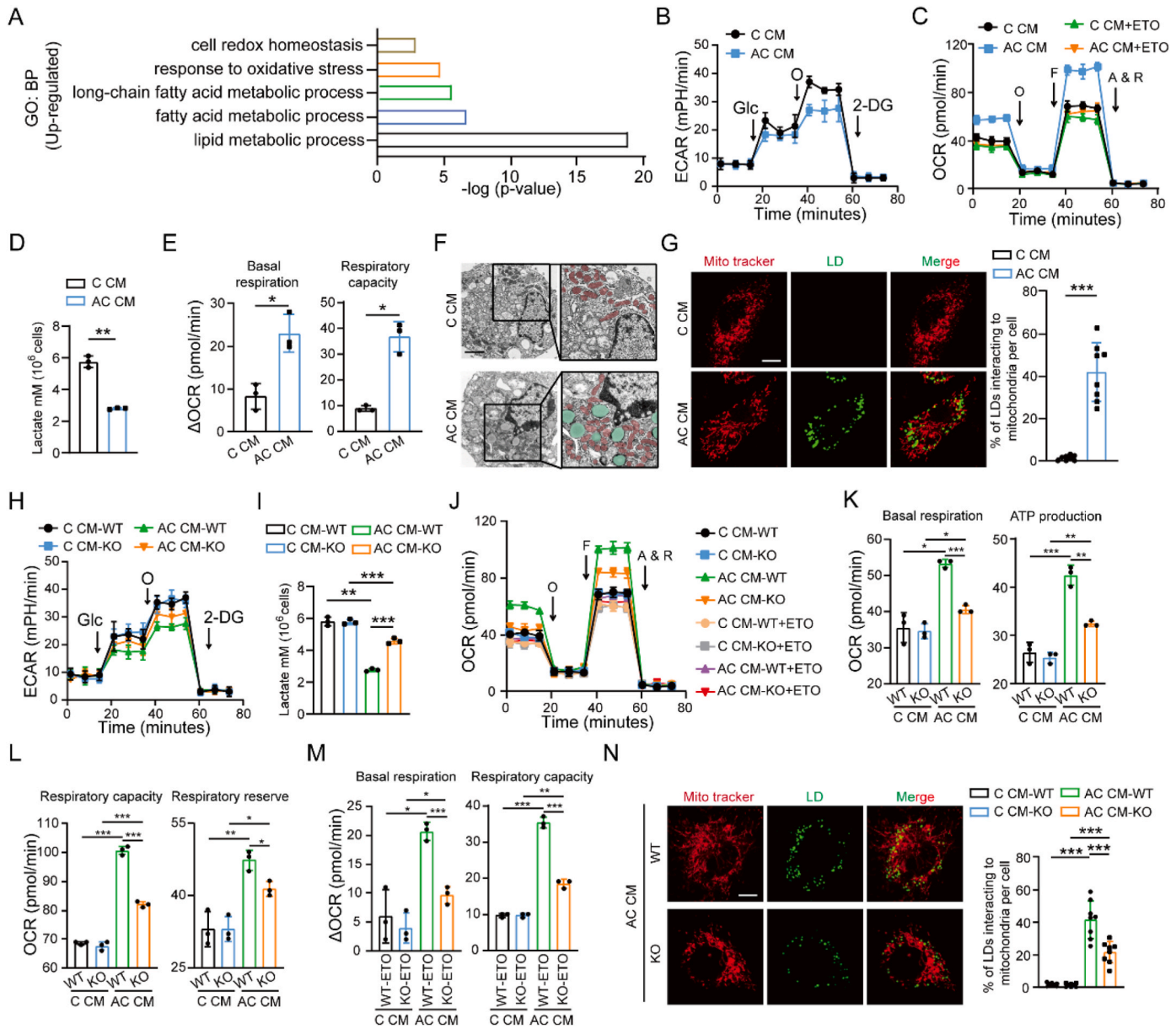

Fig. 3. Macrophages with accumulated lipids upregulate fatty acid oxidation (FAO). (A) Compared to C CM-treated BMDMs, lipid and FA metabolic processes were upregulated in AC CM-cultured BMDMs. Representative BP categories identified in GO analyses based on upregulated DEGs in AC CM-treated BDMDs compared with C CM-treated BMDMs. (B and C) The extracellular acidification rate (ECAR) (B) and oxygen consumption rate (OCR) (C) of BMDMs treated with AC CM or C CM were detected using a Seahorse Bioscience XFp analyzer (n = 3). In the measurement of ECAR, cells were sequentially treated with glucose (Glc), oligomycin (O), and 2-deoxyglucose (2-DG) (B); when OCR was detected, cells were sequentially treated with O, FCCP (F) and antimycin A/rotenone (A&R). Etomoxir (ETO, an FAO inhibitor that blocks the transport of FAs into the mitochondrion) was further used to detect FAO. (D) Lactate production in BMDMs cultured with AC CM or C CM was determined (n = 3). Values are presented as means ± s.d., **P < 0.001. (E) Results of the statistical analysis of ΔOCR of basal respiration and respiratory capacity showing that AC CM treatment facilitates FAO in macrophages (n = 3). Values are presented as means ± s.d., *P < 0.05. ΔOCR (calculated as OCR without ETO stimulation minus OCR in the ETO-stimulated group) of basal respiration and respiratory capacity were used to determine FAO fueled by FAs present in mitochondrion. (F) Representative TEM micrographs of contacts between LDs (green) and mitochondrion (red) in BMDMs cultured with AC CM or C CM. Scale bars, 10 μm. (G) The left panel shows representative confocal images of BMDMs stained with MitoTracker (red) and BODIPY 493/503 (green) after treatment with AC CM or C CM. The right panel shows the quantification of the interaction between LDs and mitochondrion. Values are presented as means ± s.d., ***P < 0.0001. Scale bars, 10 μm. (H) The ECAR of WT and MSR1 KO BMDMs cultured with AC CM or C CM was tested (n = 3). (I) Lactate secretion from BMDMs treated with AC CM or C CM was measured (n = 3). Values are presented as means ± s.d., **P < 0.001, ***P < 0.0001. (J–L) Upon treatment with AC CM or C CM, the OCR of WT and MSR1 KO BMDMs was evaluated (n = 3) (J). Furthermore, basal respiration (K), ATP production (K), respiratory capacity (L), and respiratory reserve (L) were determined in the indicated groups of BMDMs (n = 3). Values are presented as means ± s.d., *P < 0.05, **P < 0.001, ***P < 0.0001. (M) The ΔOCR of basal respiration and respiratory capacity were calculated as the response of BMDMs in the indicated groups to ETO treatment (n = 3). Values are presented as means ± s.d., *P < 0.05, **P < 0.001, ***P < 0.0001. (N) LD-mitochondrion contact in WT and MSR1 KO BMDMs treated with AC CM or C CM (Sup Fig. 3L) was evaluated by staining cells with MitoTracker (red) and BODIPY 493/503 (green) (n = 3) (left panel). These contacts were also quantified in the indicated groups (right panel). Values are presented as means ± s.d., ***P < 0.0001. Scale bars, 10 μm. (For interpretation of the references to color in this figure legend, the reader is referred to the Web version of this article.)

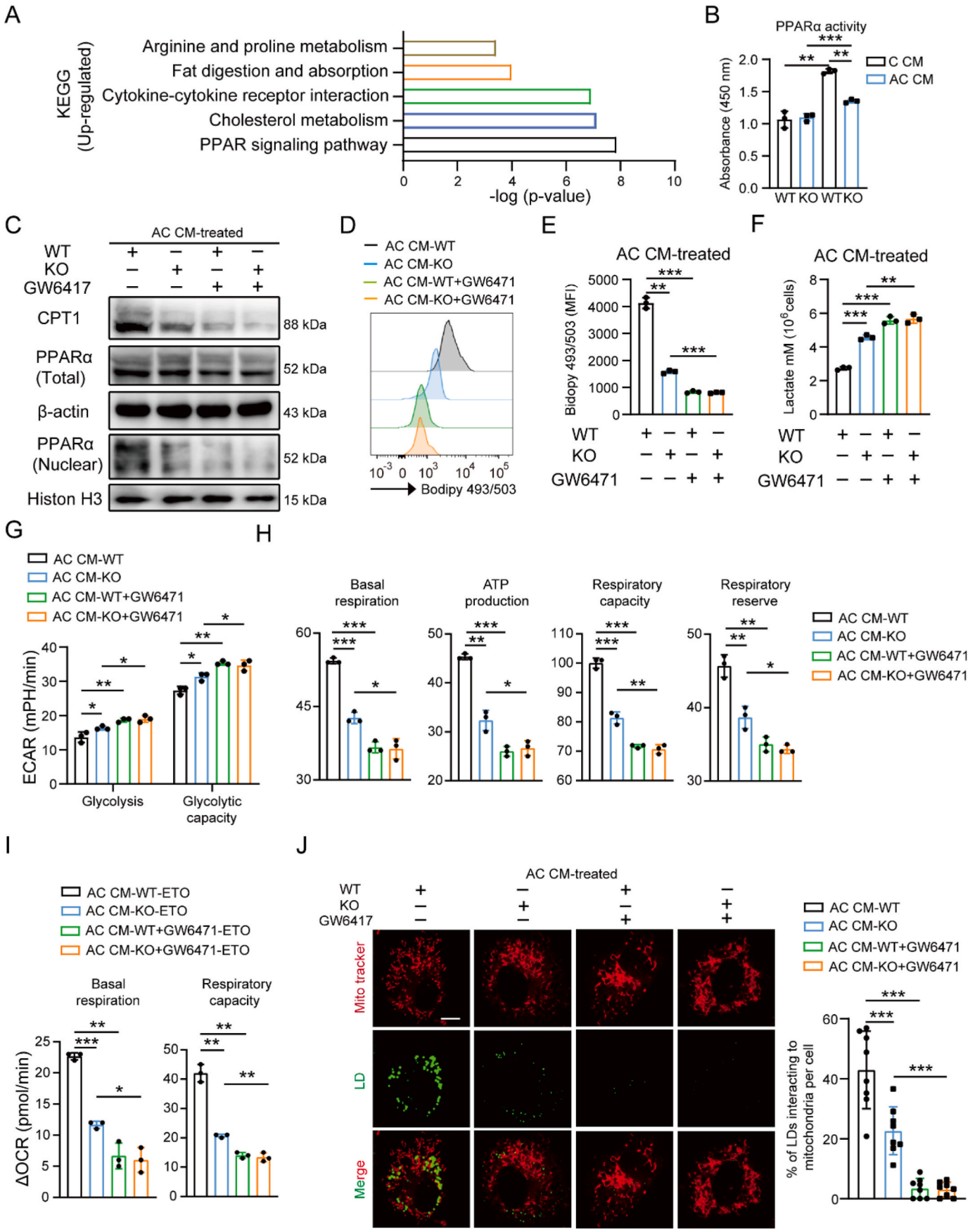

(caption on next page)

Fig. 4. PPARα activation in macrophages is required for AC CM-induced LD formation and FAO upregulation.
(A) Representative KEGG pathway categories of upregulated DEGs affected by AC CM treatment in BMDMs. (B and C) AC CM treatment activated PPARα in macrophages. PPARα activity was measured in a series of concentrations of nuclear extracts (NEs) from WT and MSR1 KO BMDMs exposed to AC CM or C CM (n = 3) (B). Values are presented as means ± s.d., **P < 0.001, ***P < 0.0001. Furthermore, levels of the CPT1, PPARα (total), β-actin, PPARα (nuclear) and Histone H3 proteins in WT and MSR1 KO BMDMs treated with AC CM or C CM (Sup Fig. 4D) were measured using western blotting (C). (D and E) Representative histograms (D) and statistical analysis of MFI (E) showing the importance of PPARα in LD formation in BMDMs treated with AC CM or C CM based on quantifying the fluorescence intensity of BODIPY 493/503 (n = 3). Values are presented as means ± s.d., **P < 0.001, ***P < 0.0001. (F) GW6471 treatment increased lactate production in WT and MSR1 KO BMDMs cultured with AC CM (n = 3). Values are presented as means ± s.d., **P < 0.001, ***P < 0.0001. (G) The administration of GW6471 promoted glycolysis, as determined by calculating the glycolysis and glycolytic capacity of WT and MSR1 KO BMDMs treated with AC CM (n = 3). Values are presented as means ± s.d., *P < 0.05, **P < 0.001. (H and I) PPARα inhibition by GW6471 decreased OXPHOS and FAO in WT and MSR1 KO BMDMs after culture with AC CM, as evidenced by basal respiration, ATP production, respiratory capacity, respiratory reserve and ΔOCR. Values are presented as means ± s.d., *P < 0.05, **P < 0.001, ***P < 0.0001. (J) The left panel shows representative confocal images of GW6471-treated WT and MSR1 KO BMDMs stained with MitoTracker (red) and BODIPY 493/503 (green) after treatment with AC CM. In the right panel, the interactions between LDs and MitoTracker in BMDMs from the indicated groups were quantified. Values are presented as means ± s.d., ***P < 0.0001. Scale bars, 10 μm.

substantially inhibited by an anti-BMP7 monoclonal antibody. Furthermore, the mRNA expression patterns of the osteogenic markers *col1*, *alp*, *ocn* and *runx2* on day 7 and day 14 in the indicated groups also supported the crucial role of BMP7 (Fig. 6G and H). Taken together, these data suggest that FAO-dependent BMP7 production may be closely associated with the osteogenic differentiation of BMSCs induced by macrophages in response to AC CM.

2.7. The NAD^+/SIRT1/EZH2 axis controls BMP7 expression in macrophages after treatment with AC CM

Next, we intended to elucidate the in-depth mechanism by which FAO controls BMP7 expression in macrophages. An increase in mitochondrial FAO is associated with electron transport and OXPHOS, and the cofactor NAD^+ plays a key role in providing electrons for complex I (CI) of the electron transport chain (ETC) to drive OXPHOS [24,25]. Moreover, decreases in NAD^+ levels lead to a loss of ETC activity in macrophages [26]. Given the importance of NAD^+ in the ETC, we speculated that an increased NAD^+ level is required for elevated FAO in macrophages in response to AC CM. As expected, NAD^+ levels in AC CM-treated BMDMs were substantially increased compared with those in C CM-treated BMDMs (Sup Fig. 6A). However, knockout of MSR1 in BMDMs after culture with AC CM and inhibition of PPARα or CPT1A significantly decreased NAD^+ levels (Fig. 7A). Sirtuins (SIRTs) are classically considered as the main consumers of NAD^+ through their enzymatic reactions [27]. Then, siRNAs targeting selected SIRT families, such as SIRT1, SIRT2, SIRT3, SIRT5, SIRT6 and SIRT7 (due to their regulatory effect on bone biology) were used to detect whether the expression of BMP7 was affected (Sup Fig. 6B) [28–34]. As shown in Sup Fig. 6C, compared with the control group, only siRNA-mediated silencing of SIRT1 affected *bmp7* expression. NAD^+ is a reported regulator of SIRT1, which supports its deacetylase activity [35]. Next, we detected decreased levels of proteins with acetylated lysine residues in AC CM-treated BMDMs compared with those cultured with C CM (Sup Fig. 6D). In addition, more intense bands of lysine-acetylated proteins were observed in MSR1 KO BMDMs than in WT BMDMs after treatment with AC CM (Sup Fig. 6D). Further validation experiments suggested that SIRT1 protein activity was increased in BMDMs treated with AC CM compared with C CM, and MSR1 deficiency and treatment with GW6471 and ETO significantly decreased the elevated SIRT1 activity observed in BMDMs treated with AC CM (Fig. 7B and Sup Fig. 6E).

Then, we asked whether FAO-modulated NAD^+/SIRT1 activity is associated with BMP7 generation in macrophages after culture with AC CM. As shown in Fig. 7C and Sup Fig. 6F, after replenishing the NAD^+ precursor NMN, BMP7 mRNA and protein levels were both restored in MSR1 KO BMDMs treated with AC CM. However, BMP7 expression was substantially decreased in BMDMs treated with EX527 (a SIRT1 inhibitor) (Fig. 7C and Sup Fig. 6F). Notably, because SIRT1 activity is downstream of NAD^+, EX527-treated BMDMs were refractory to BMP7 rescue after supplementation with NMN (Fig. 7C and Sup Fig. 6F). We focused on epigenetic mechanisms to assess mechanistic links between NAD^+/SIRT1 activity and *bmp7* gene expression. Based on a public database (https://www.genecards.org), 109 TFs were predicted to regulate *bmp7* expression (Fig. 7D). Among them, 14 TFs were reported to be deacetylated by SIRT1 in a literature review (Fig. 7D) [36–49]. However, only 4/14 TFs (Enhancer Of Zeste 2 Polycomb Repressive Complex 2 Subunit [EZH2], CCAAT Enhancer Binding Protein Alpha [CEBPA], Forkhead Box A2 [FOXA2] and Forkhead Box A3 [FOXA3]) that were deacetylated by SIRT1 positively modulated the expression of target genes (Fig. 7D). Thus, we explored the role of these four TFs (EZH2, CEBPA, FOXA2 and FOXA3) in regulating *bmp7* expression by transfecting cells with small interfering RNAs (siRNAs) to obtain further insights into the molecular mechanism (Sup Fig. 6G). Compared with the control group, only siRNA-mediated silencing of EZH2 exerted a regulatory effect on *bmp7* (Sup Fig. 6H). EZH2, which is deacetylated by SIRT1, epigenetically regulates the expression of genes by trimethylating histone 3 at lysine 27 (H3K27me3) [50]. Hence, we hypothesized that MSR1-mediated FA uptake triggers FAO, which further increases the activity of NAD^+/SIRT1, leading to decreased levels of acetylated EZH2 with methyltransferase activity and the subsequent induction of target gene expression (Fig. 7E). Consistent with our hypothesis, downregulation of FAO via MSR1 deficiency and GW6471 or ETO treatment decreased *bmp7* expression (Sup Fig. 5I and J) and increased the acetylation of EZH2 and the levels of H3K27me3 (Fig. 7F and G). Furthermore, the levels of the acetylated EZH2 protein and H3K27me3 were reduced in AC CM-treated MSR1 KO BMDMs after supplementation with NMN (Fig. 7H and I and Sup Fig. 6I). However, higher levels of acetylated EZH2 and H3K27me3 were observed in the presence of EX527 (Fig. 7H and I and Sup Fig. 6I). When we compared callus-sorted macrophages on day 7 and day 14 post fracture, macrophages exhibited higher MSR1 expression and lower levels of H3K27me3 on day 14 than on day 7 (Fig. 7J-L). Based on these data, MSR1 decreases the methyltransferase activity of EZH2 as a consequence of increased levels of NAD^+ and upregulation of SIRT1 deacetylase activity.

We next determined whether EZH2 epigenetically regulates BMP7 expression via H3K27me3. Bioinformatics analyses using integrative genomics viewer (IGV) revealed a common potential binding site for EZH2 and H3K27me3 in the regulatory regions of BMP7 (Sup Fig. 6J). Subsequently, chromatin immunoprecipitation (ChIp)-qPCR was performed to verify the binding of EZH2 and H3K27me3 to the selected region of BMP7 in BMDMs treated with AC CM or C CM. As indicated in Fig. 7M and N, EZH2 and H3K27me3 binding to BMP7 loci was observed in both AC CM and C CM-stimulated BMDMs, but stronger binding signals were detected in C CM-treated BMDMs, suggesting that the transcriptionally repressive effect of EZH2 on catalyzing the H3K27me3 modification is significantly diminished in BMDMs treated with AC CM. Thus, these results revealed that the NAD^+/SIRT1/EZH2 axis is required for FAO-mediated BMP7 expression in macrophages cultured with AC CM.

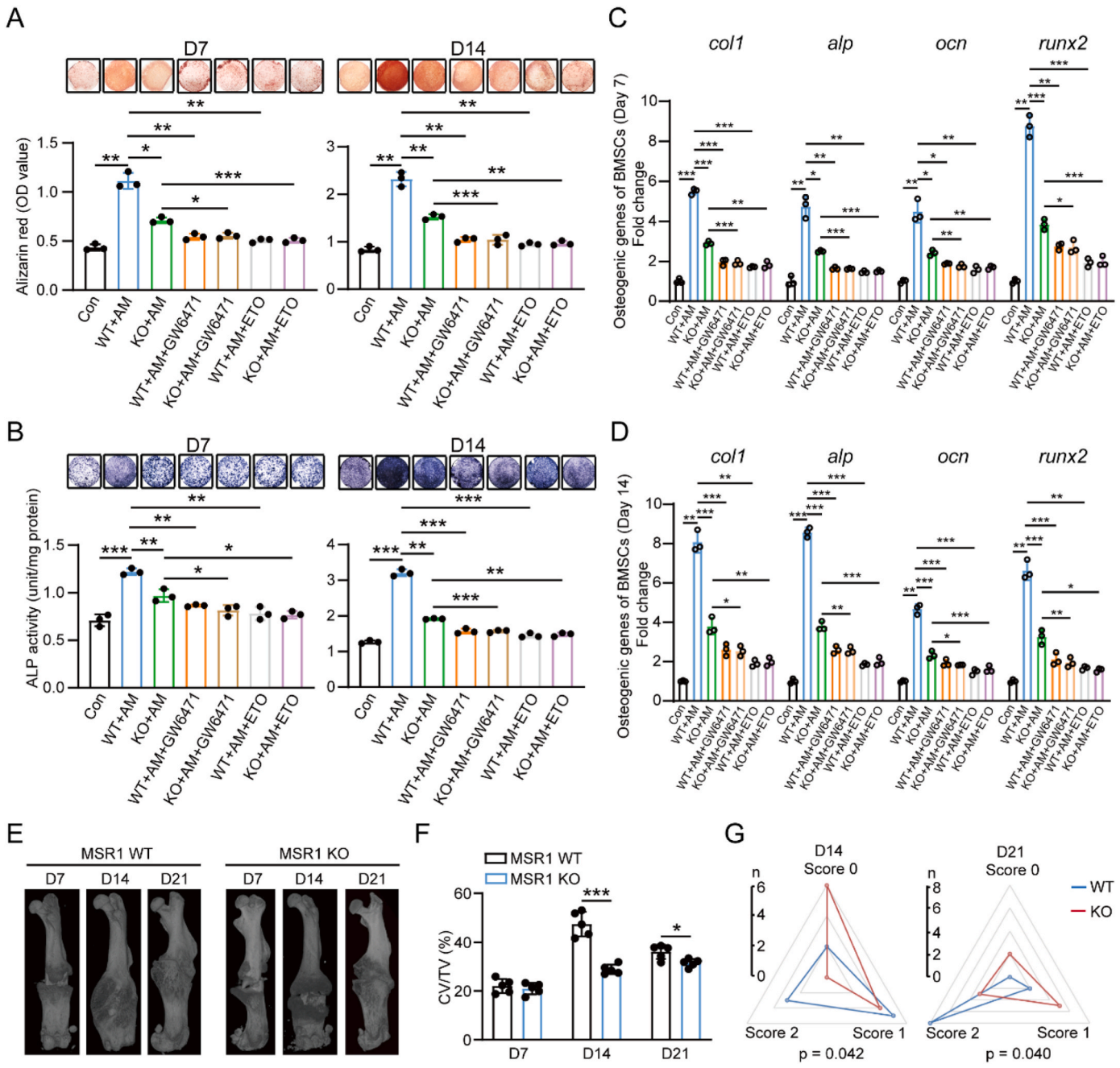

Fig. 5. Attenuating FAO in macrophages decreased the pro-osteogenic differentiation activity of macrophages.
(A and B) BMSCs were cultured in osteogenesis induction medium plus CM from AC CM-treated WT or MSR1 KO BMDMs, as indicated. BMSCs cultured with osteoblast differentiation medium alone were regarded as the control group. After 7 and 14 days, matrix mineralization was tested by performing alizarin red (AR) staining (upper panel of A) and ALP staining (upper panel of B). Quantitative analyses of AR staining (lower panel of A) and ALP activities (lower panel of B) on D7 and D14 are shown. Values are presented as means ± s.d., *P < 0.05, **P < 0.001, ***P < 0.0001. AM = Apoptotic chondrocyte CM. (C and D) After 7 (C) and 14 (D) days, mRNA expression patterns of osteoblast-specific marker genes (Col1, Alp, Ocn, and Runx2) in the indicated groups were determined using RT–qPCR. β-Actin was used as an internal control. Values are presented as means ± s.d., *P < 0.05, **P < 0.001, ***P < 0.0001. AM = Apoptotic chondrocyte CM. (E and F) The importance of MSR1 during EO *in vivo* was evaluated using a femoral fracture model. Representative 3D images of micro-CT scans from WT and MSR1 KO mice on D7, D14 and D21 post fracture (E). Statistical analysis of mineralized callus volume/tissue volume (CV/TV, %) from micro-CT scans (F). Each group contained five animals. Values are presented as means ± s.d., *P < 0.05, ***P < 0.0001. (G) Representative X-ray images of WT and MSR1 KO mice at D14 and D21 after fracture were captured (Sup Fig. 5E), and the quantification of these images revealed significantly lower union rates in MSR1 KO mice at D14 and D21 post fracture (n = 10, Chi-square test).

2.8. The beneficial therapeutic effects of AC CM administration and targeting MSR1 expressed in macrophages on bone regeneration in vivo

In contrast to the repair process in the femoral fracture model, the formation of new bone without a cartilaginous intermediary accounts for bone defect repair in the tibial monocortical defect model [2]. Thus, we examined the significance of our findings obtained using AC CM by measuring bone regeneration in a tibial monocortical defect model treated with AC CM or C CM *in vivo*. As indicated in Fig. 8A–E, the administration of AC CM resulted in better new bone formation,

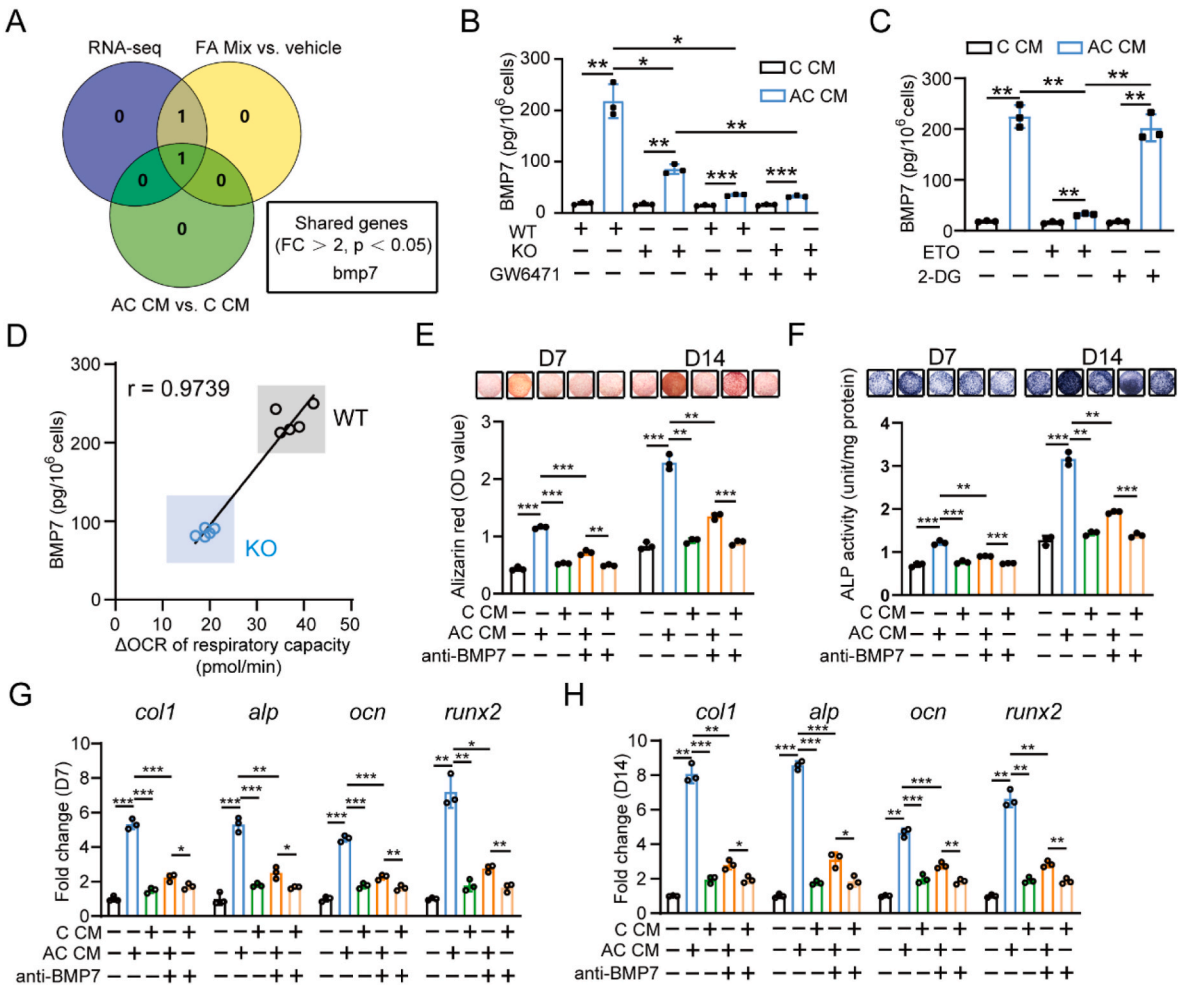

Fig. 6. AC CM-treated macrophages promote BMSC osteogenic differentiation by increasing FAO-regulated BMP7 production.
(A) Venn diagram depicting bmp7 as the only overlapping significantly upregulated chemokine among the three lists (List 1: DEGs of the bmp family from the RNA-seq data; List 2: significantly upregulated bmp family genes in FA mix-treated BMDMs compared to control cells; List 3: significantly upregulated bmp family genes in AC CM-stimulated BMDMs compared to C CM-treated BMDMs). (B and C) The amount of secreted BMP7 in C CM- or AC CM-cultured WT and MSR1 KO BMDMs treated with or without GW6471 (PPARα inhibitor) (B), ETO (CTP1A inhibitor) (C) or 2-DG (glycolysis inhibitor) (C) was evaluated using ELISA (n = 3). The results are presented as the means ± s.d., *P < 0.05, **P < 0.001, ***P < 0.0001. (D) The correlation between BMP7 production and ΔOCR of respiratory capacity in BMDMs from WT and MSR1 KO mice is shown (n = 5 mice/genotype). r indicates Pearson's correlation coefficient (r = 0.9739). (E and F) Representative images (upper panel) and statistical analysis (lower panel) of AR staining (E) and ALP staining (F) in BMSCs from the indicated groups on D7 and D14 suggest a crucial role for BMP7. The results are presented as the means ± s.d., **P < 0.001, ***P < 0.0001. (G and H) After 7 (G) and 14 (H) days, mRNA expression patterns of osteoblast-specific marker genes (Col1, Alp, Ocn, and Runx2) in the indicated groups were tested using RT–qPCR and further suggested that BMP7 might be closely associated with the osteogenic differentiation of BMSCs induced by macrophages treated with AC CM. The results are presented as the means ± s.d., *P < 0.05, **P < 0.001, ***P < 0.0001.

significantly increased trabecular bone volume/total volume (BV/TV) and trabecular number (Tb.N), and a decreased trabecular separation (Tb.Sp), compared with animals treated with or without C CM. Moreover, we tested the osteoinductive effect using FA mix. FA mix also induced more newly formed bone tissue, as determined using micro-CT scanning. Calculations of morphometric parameters showed significantly increased BV/TV and Tb.N, and a decreased Tb.Sp in mice treated with FA mix compared with the vehicle controls (Sup Fig. 7A–E). Next, clodronate liposomes (macrophage depletion) were used to determine whether macrophages contributed to the enhanced bone regeneration during bone defect repair in response to AC CM. The efficiency of monocyte/macrophage depletion was first verified using a flow cytometry assay (Sup Fig. 7F). The 3D reconstructed images and morphometric parameters consistently suggested that the enhanced bone regeneration was mostly attributed to macrophages after treatment with AC CM (Fig. 8A–E). As MSR1-mediated FA uptake in macrophages is the main factor contributing to the interaction between AC CM and macrophages, bone marrow transplantation (BMT) assays were conducted in which irradiated MSR1 KO mice were reconstituted with bone marrow from either MSR1 KO or WT mice to further confirm the link between macrophage MSR1 and EO. Compared with the appropriate control mice, the micro-CT images and quantification of CV/TV both revealed better EO on day 14 and day 21 post fracture in MSR1 KO mice transplanted with MSR1 WT bone marrow (Fig. 8F and G). Additionally, compared to the control group, X-rays from irradiated MSR1 KO mice reconstituted with bone marrow from WT mice displayed increased union rates on day 14 and day 21 post fracture (Fig. 8H and Sup Fig. 7G). Taken together, utilization of AC CM and targeting macrophage MSR1 can be harnessed to exert beneficial effects in bone regeneration *in vivo*.

3. Discussion

Although accumulating evidence indicates that macrophages are needed for EO during fracture repair, the specific contribution and

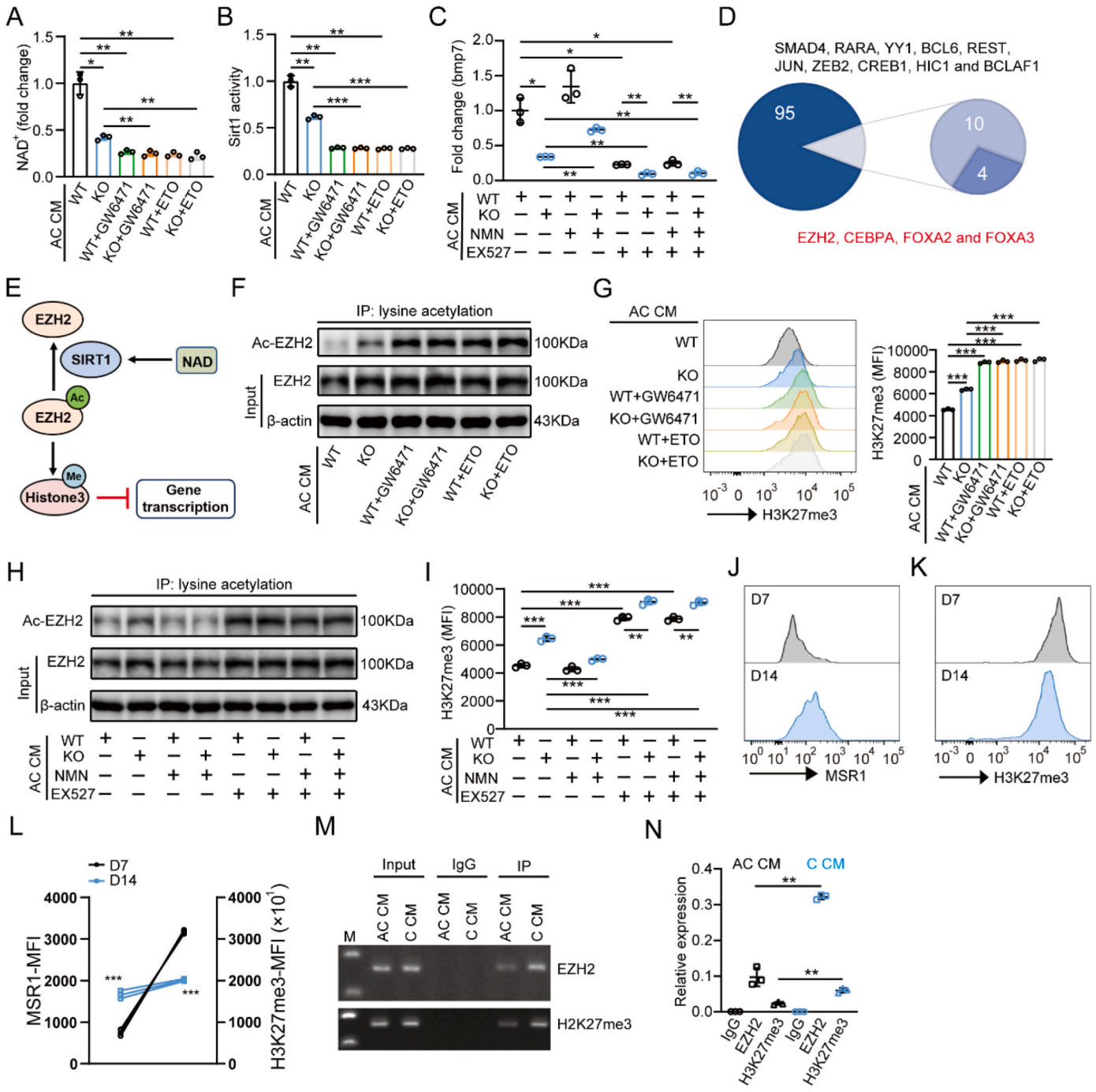

Fig. 7. BMP7 production by macrophages in response to AC CM is regulated by the NAD^+/SIRT1/EZH2 axis

(A) The level of NAD^+ quantified by colorimetric measurements indicated that the loss of MSR1 and inhibition of PPARα or CPT1A significantly reduced the NAD^+ level in BMDMs cultured with AC CM (n = 3). Values are presented as means ± s.d., *P < 0.05, **P < 0.001. (B) SIRT1 protein activity was measured in AC CM-stimulated WT and MSR1 KO BMDMs treated with or without GW6471 or ETO (n = 3). Values are presented as means ± s.d., **P < 0.01, ***P < 0.0001. (C) NMN (NAD^+ precursor) supplementation partially rescues the bmp7 mRNA level in MSR1 KO BMDMs, but not EX527-treated BMDMs (an inhibitor of SIRT1) (n = 3). Values are presented as means ± s.d., *P < 0.05, **P < 0.001. (D) Based on a public database and our literature review, 4/109 TFs (EZH2, CEBPA, FOXA2 and FOXA3) deacetylated by SIRT1 are presumed to positively modulate the expression of target genes. (E) Schematic showing the regulatory mechanism of gene transcription by the NAD^+/SIRT1/EZH2 axis. (F) Cell lysates from WT and MSR1 KO BMDMs treated with or without GW6471 or ETO were subjected to immunoprecipitation with an EZH2 antibody followed by Western blot analysis with antibodies against acetylated lysine or EZH2. (G) Representative histograms (left panel) and statistical results (right panel) displaying the level of H3K27me3 in WT and MSR1 KO BMDMs cultured in the presence or absence of GW6471 or ETO and detected using flow cytometry (n = 3). Values are presented as means ± s.d., ***P < 0.0001. (H) The level of acetylated EZH2 in AC CM-treated WT and MSR1 KO BMDMs from the indicated groups was detected using western blotting with acetyl-lysine or EZH2 antibodies. (I) The level of H3K27me3 in AC CM-treated WT and MSR1 KO BMDMs from the indicated groups was determined using flow cytometry (n = 3). Values are presented as means ± s.d., **P < 0.001, ***P < 0.0001. (J–L) Representative histograms and statistical analysis of MFI (L) showing the levels of MSR1 (J and L) and H3K27me3 (K and L) in callus-sorted macrophages from the TZ on D7 and D14 post fracture. Values are presented as means ± s.d., ***P < 0.0001. (M and N) A ChIP-qPCR assay of BMDMs cultured with AC CM or C CM was performed to verify the potential binding site for EZH2 and H3K27me3 in the BMP7 promoter region. Integration maps of the ChIP assay are shown (M). IgG and input fractions were used as controls. A statistical analysis of qPCR was also conducted (N). Values are presented as means ± s.d., **P < 0.001.

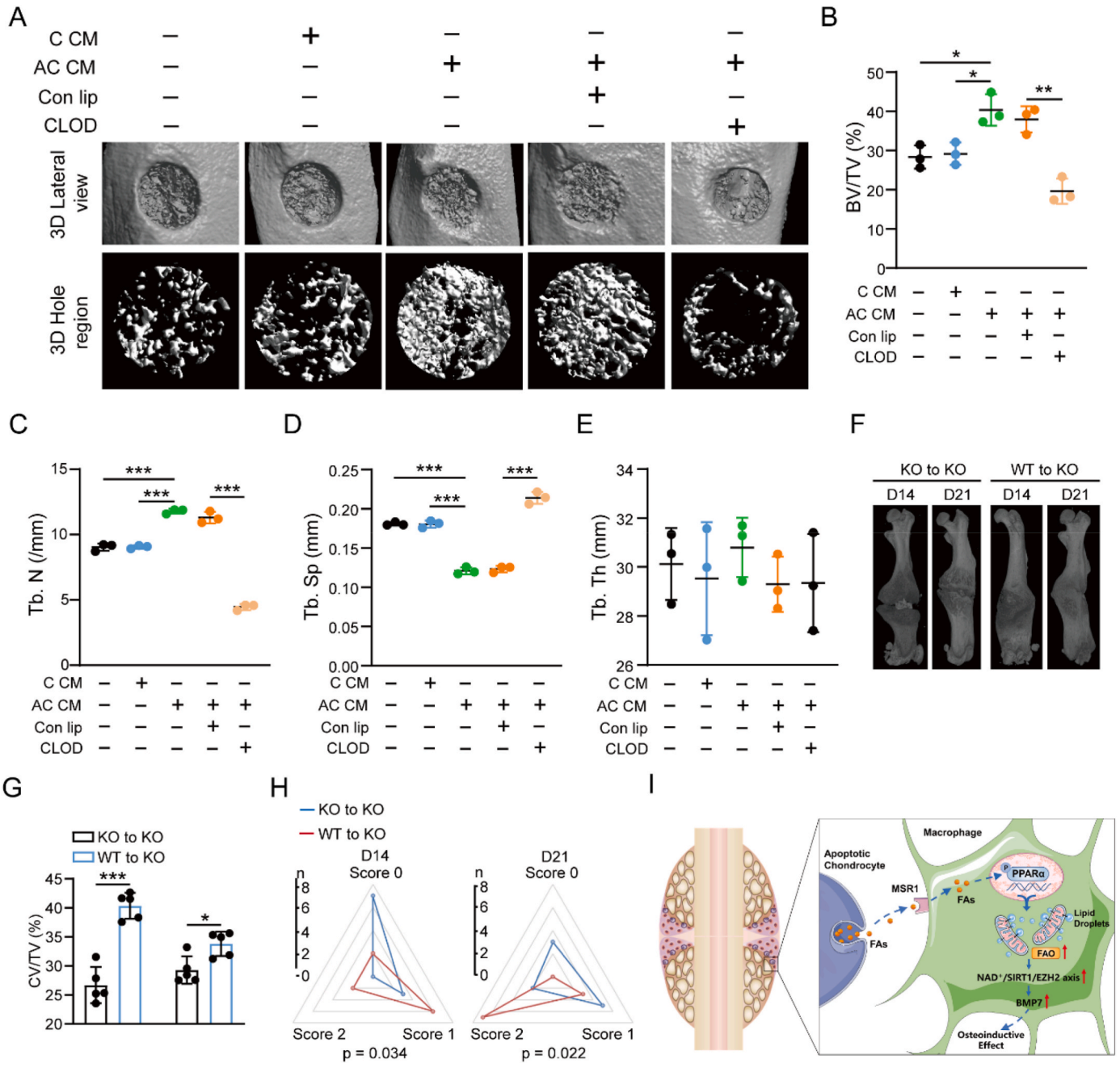

Fig. 8. Administration of AC CM and targeting macrophage MSR1 facilitate bone regeneration *in vivo*.
(A) The effect of AC CM on bone regeneration *in vivo* was assessed using a tibial monocortical defect model. The increased bone regeneration observed in the AC CM-treated group was largely diminished when CLOD (depletion of macrophages) was administered. Representative micro-CT images of the reconstruction of injured tibias (upper panel) and mineralized callus tissues (lower panel) in the defect area of the indicated groups. CLOD: clodronate liposomes. (B–E) Statistical analysis of bone volume/total volume (BV/TV) (%) (B), trabecular number (Tb.N) (C), trabecular separation (Tb.Sp) (D), and trabecular thickness (Tb.Th) (E) of the mineralized bone formed in the hole region (n = 3). The results are presented as the means ± s.d., *P < 0.05, **P < 0.001, ***P < 0.0001. (F and G) Representative micro-CT images (G) and statistical analysis of CV/TV (H) both suggested that compared to the better repair in the appropriate control group, endochondral ossification occurred during fracture repair on D14 and D21 post fracture in MSR1 KO mice transplanted with MSR1 WT bone marrow. The results are presented as the means ± s.d., *P < 0.05, ***P < 0.0001. (H) Representative X-ray images and quantification indicated that compared to control mice, irradiated MSR1 KO mice reconstituted with bone marrow from MSR1 WT mice showed higher union rates on D14 and D21 post fracture (n = 10, Chi-square test). (I) Schematic of the functional consequences and specific mechanism of AC-released FAs in macrophages during EO. As we indicated, ACs and macrophages were observed in the TZ. FAs derived from ACs are taken up by macrophages mainly through MSR1, which modifies the intracellular level of FAs and activates PPARα. Then, LD formation and FAO activity are increased by PPARα activation and subsequently increase the level of NAD^+. Furthermore, the NAD^+/SIRT1/EZH2 axis positively regulates bmp7 expression, which accounts for the osteoinductive effect of macrophages treated with AC CM.

mechanism of macrophages to the mineralization process transforming cartilage into woven bone are still largely unknown. Notably, the data from this study and others revealed a group of macrophages adjacent to ACs in the TZ, which represents a unique chondro-osseous junction. Furthermore, the most significant finding of the present study is that ACs modulate the pro-osteogenic differentiation property of macrophages by releasing FAs. As shown in Fig. 8I, FAs derived from ACs were taken up by macrophages mainly through MSR1. Subsequently, intercellular LD formation and FAO activity were increased via PPARα activation. Moreover, due to elevated macrophage FAO, activation of the NAD^+/SIRT1/EZH2 axis was shown to increase *bmp7* expression, which facilitates the osteogenic differentiation of BMSCs. Overall, our findings provide a novel functional and mechanistic basis for the interplay between ACs and macrophages during EO.

Traditionally, chondrocytes mature to hypertrophy and undergo apoptosis, and new bone is generated by invading MSCs during EO of fracture repair [2,51]. Consistent with previously published data, our work also confirmed that the rate of chondrocyte apoptosis increased during fracture repair. Furthermore, our study documented a previously unrecognized role for AC-mediated metabolic and functional reprogramming in macrophages. Notably, in addition to the classic EO concept, three other models of the transdifferentiation of chondrocytes to osteoblasts (chondrocyte to osteogenic precursor model, dedifferentiation to redifferentiation model and direct transdifferentiation model) have recently been proposed, and each of them is mechanistically different [5]. We are inclined to agree with the viewpoint that transdifferentiation models working in conjunction with canonical EO models promote bone regeneration and that each model might exhibit a specific temporal and spatial pattern.

Given the importance of apoptosis in development and homeostatic tissue turnover, an advanced concept suggests that apoptotic cells remain intact for a period of time and release certain metabolites that diffuse within a tissue to influence neighboring cells [9]. To the best of our knowledge, we are the first to show that FAs derived from ACs affect macrophage functions during EO. Scavenger receptors (MSR1, CD36, CD68 and MARCO) are a group of crucial phagocytic receptors responsible for the uptake of FAs in macrophages. In this study, we confirmed that AC CM increased MSR1 expression and that knockout of MSR1 significantly inhibited the uptake of FAs and FAO activity. Based on our results, during the interplay between ACs and macrophages in EO, MSR1 expressed on macrophages is a key receptor for FA uptake, which also represents an initiating factor for elevated FAO. Notably, MSR1 is reported to endocytose heterogeneous substances and participate in intracellular signaling [11]. Considering the complexity of AC and AC CM, apart from FAs, other components may also regulate the function of macrophages. Further studies are needed to determine whether other ligands of MSR1 are released from ACs and how they regulate the function of macrophages during EO.

Recent studies have focused on the metabolic disparity among macrophages activated by diverse stimuli in a specific microenvironment. Intracellular metabolic rewiring is a critical hallmark of macrophage activation [52]. M1-like macrophages require a high level of glycolysis to fulfill their cytocidal functions, whereas M2-like macrophages are considered to employ increased mitochondrial OXPHOS to promote tissue repair [52]. In addition, Lipid metabolism in macrophages has attracted increasing attention because it provides an anti-inflammatory function and accelerates the healing of bone defects [24]. However, little information is available about the metabolic characteristics of macrophages during EO. In our study, compared with C CM-cultured macrophages, AC CM-treated macrophages exhibited decreased glycolysis and increased FAO, which facilitated their osteoinductive function. Interestingly, another study also indicated that increased FAO in macrophages was involved in their wound repair functions by supporting IL-10 generation [53]. Although FAO is reported to be crucial for the proinflammatory effect of macrophages under certain circumstances, based on our results, targeting FAO in macrophages during EO might be a promising therapeutic method for fracture repair.

In this study, we explored the mechanism underlying the increased production of *bmp7* in AC CM-stimulated macrophages and found that the NAD^+/SIRT1/EZH2 axis was responsible for this effect. SIRT1 is an NAD^+-dependent deacetylase that is conserved from bacteria to humans. Cell biological studies have further shown that NAD^+-SIRT1 is a promising regulator of bone remodeling, including maintaining bone-forming cell viability and attenuating bone resorption [29]. However, the effect of macrophage-derived SIRT1 on fracture repair is currently unknown. Furthermore, Casarin et al. revealed that the beneficial effects of resveratrol (an agonist targeting SIRT1) on the repair of bone defects are mediated by upregulating the mRNA expression of *bmp7*, *bmp2* and *opn* [54]. However, the specific regulatory mechanism has not been determined. EZH2, a histone methyltransferase, catalyzes H3K27me3 to negatively regulate gene expression [55]. Several studies have highlighted the role of EZH2 in skeletal development and homeostasis [56]. Inhibition of EZH2 promotes BMSC osteogenesis, skeletal development, and postnatal bone remodeling [56]. Recently, a number of studies have indicated that deacetylation of EZH2 by the deacetylase SIRT1 decreases its capacity to suppress the expression of target genes [49,50]. In our study, EZH2 deacetylation by SIRT1 was proven to upregulate the expression of *bmp7* in macrophages treated with AC CM.

We provide insights into the functional consequences and specific mechanisms of AC-produced FAs in macrophages during EO. Our works, together with other researches demonstrated that MSR1-mediated PI3K/AKT signaling, PPARα signaling, NF-κB signaling, etc. might be pathways activated in macrophages adapting to different microenvironmental signals [14,57]. However, an identifiable limitation of this study is that the contributions of individual FAs derived from ACs in macrophages were not tested. It is also worth noting that, apart from the LCFAs, the short-chain FAs (SCFAs) also have been proved to exert a regulatory effect on macrophage polarization and bone mass [58,59]. Due to the complexity surrounding FAs and fracture repair, the formation of a definite conclusion concerning the effect of FAs on fracture healing is premature. In this study, we focused on the functional consequences of FAs derived from ACs, and the potential mechanism of FA release in ACs requires further analysis. Moreover, whether ACs and macrophage MSR1 contribute to fracture healing in patients needs further study.

Overall, our study advanced the concept that ACs are not inert corpses awaiting removal, but positively regulate bone regeneration by releasing FAs. The data from our functional experiments further confirmed that exogenous FAs derived from ACs are taken up by macrophages mainly through MSR1. This is a prerequisite and crucial step for mediating the subsequent activation of PPARα, which further facilitates LD generation and FAO. Moreover, we elucidated a previously undescribed role of FAO in regulating the osteoinductive effect and showed that the NAD^+/SIRT1/EZH2 axis effectively increased the expression of *bmp7* in macrophages cultured with AC CM. Thus, macrophages represent a viable target for fracture treatments with a potentially broad therapeutic window, and MSR1 expressed in macrophages can be targeted as a therapeutic approach for enhancing fracture repair.

4. Materials and methods

4.1. Apoptosis induction and validation

Primary chondrocytes isolated from 5-day-old mice were treated with staurosporine (1 μM) for 6 h to induce apoptosis. Living chondrocytes were used as the control group. Then, these chondrocytes were stained with FITC-Annexin V and propidium iodide and subjected to flow cytometry. Data were analyzed using FlowJo v.10 software, and approximately 90% of the chondrocytes were apoptotic. To get conditioned medium, we incubated the ACs for another 4 h in DMEM/F-12

supplemented with 10% FBS and a 1% antibiotic mixture following washing. Afterward, the cell medium was obtained by centrifugation at 13,000 g for 10 min and then filtered through 0.2 mm pore filters to remove apoptotic bodies [60]. The clarified culture medium (CM) from ACs was termed AC CM, and CM from control chondrocytes was termed C CM.

4.2. C12 transfer assays

Chondrocytes were first incubated with the corresponding CM containing 2 μM BODIPY 558/568C12 (D3835, Thermo Fisher Scientific, USA) for 16 h and apoptosis was induced by applying staurosporine (HY-15141, MCE, USA). Then, chondrocytes were gently washed three times with warm PBS and incubated for an additional 12 h in complete medium. AC CM was collected, and BMDMs, chondrocytes, BMSCs, osteoblasts and osteoclasts were separately incubated with AC CM for 12 h. Afterward, the cells were fixed with 4% paraformaldehyde for 30 min and stained with 500 ng/ml BODIPY 493/503 in PBS for 15 min at room temperature in the dark. Imaging was performed with a confocal microscope (Zeiss LSM710, Heidenheim, Germany) and analyzed using ImageJ software (NIH, USA).

4.3. Flow cytometry analysis of H3K27me3

Macrophages were first fixed and permeabilized using a transcription factor staining buffer set (00-5523-00, Thermo Fisher Scientific, USA) and stained to assess the levels of H3K27me3 using an Alexa Fluor 674-conjugated anti-H3K27me3 antibody (12158, CST, USA) diluted 1:300. Data were acquired using a flow cytometer (FACSVerse 8, BD) and analyzed using FlowJo software (Version 7.6.1, Treestar, USA).

4.4. Measurement of cellular energy metabolism

Energy metabolism (glycolysis, OXPHOS and FAO) in macrophages from the indicated groups was determined using the XF96 Metabolic Flux Analyzer (Seahorse Biosciences, Billerica, MA, USA) according to the manufacturer's instructions. BMDMs from the indicated groups were cultured in an XF96-well plate at a density of 1×10^4 cells per well and allowed to attach overnight. For the quantification of the ECAR, cells were sequentially incubated with 10 mM glucose, 1 μM oligomycin and 50 mM 2-deoxyglucose [61]. The O_2 consumption rate (OCR) was assessed by sequentially injecting 2 μM oligomycin, 1 μM carbonyl cyanide 4-(trifluoromethoxy) phenylhydrazone (FCCP), 1 μM antimycin A, and 1 μM rotenone (A&R) [14]. To measure the level of mitochondrial FAO, Cells were first cultured in substrate-limited medium (DMEM, 0.5 mM glucose, 1 mM GlutaMAX, 0.5 mM carnitine, and 1% FBS) overnight, and the medium was exchanged with FAO medium (DMEM, 2.5 mM glucose, 0.5 mM carnitine, and 5 mM HEPES) 45 min before the start of the OCR calculation to measure the mitochondrial FAO level. ETO (100 μM) (inhibitor of FA transport into the mitochondrial membrane) was added to the medium 15 min before the experiment [62]. Flux data were quantified using XFe Wave software (Seahorse Biosciences, California, USA). Additionally, glycolysis, the glycolytic capacity, basal respiration, ATP production, respiratory capacity (maximal ETC activity), and respiratory reserve (flexibility with increased energy demand) were all calculated according to the manufacturer's protocol. Furthermore, in this study, FAO was determined by calculating the ΔOCR of basal respiration (basal respiration $OCR_{before\ ETO} - OCR_{after\ ETO}$) and the ΔOCR of respiratory capacity (maximum respiration $OCR_{before\ ETO} - OCR_{after\ ETO}$).

4.5. Lipidomic study

Metabolites were detected and analyzed by LipidALL Technologies Co., Ltd. (Changzhou, China). FFAs were extracted from the mouse callus tissues at two different time points using a modified version of the method described previously by Bligh and Dyer to perform a lipidomic analysis of callus tissues around the TZ on day 7 and day 14 post fracture. Briefly, tissues were homogenized in 750 μl of chloroform: methanol 1:2 (v/v) with 10% deionized water and incubated at 4 °C for 30 min. At the end of the incubation, 350 μl of deionized water and 250 μl of chloroform were added. The samples were then centrifuged, and the lower organic phase containing lipids was extracted into a clean tube. Lipid extraction was carried out twice, and the lipid extracts were pooled into a single tube and dried in a SpeedVac under OH mode. Samples were stored at −80 °C until further analysis. Free FAs were analyzed using an Agilent 1290 UPLC coupled with a triple quadrupole/ion trap mass spectrometer (6500 Plus Qtrap; SCIEX) as described previously. Lipids were separated by normal phase (NP)-HPLC using a Phenomenex Luna 3 μm silica column (internal diameter 150 × 2.0 mm) under the following conditions: mobile phase A (chloroform: methanol: ammonium hydroxide, 89.5:10:0.5) and mobile phase B (chloroform: methanol: ammonium hydroxide: water, 55:39:0.5:5.5). Free FAs were quantitated using d31–16:0 (Sigma–Aldrich) and d8-20:4 (Cayman Chemicals) as internal standards.

Next, the lipidomic analysis of AC CM compared with C CM was performed by extracting FAs from mouse chondrocyte supernatant from the indicated groups (1 ml) in 10 ml glass tubes using a modified version of protocol reported by Bligh and Dyer. The lower organic phase containing FAs was dried and subjected to subsequent analyses. Free FAs (C14–C22) were analyzed using an Agilent 1290 UPLC coupled with a triple quadrupole/ion trap mass spectrometer (6500 Plus Qtrap; SCIEX) as described previously. Lipids were separated by normal phase (NP)-HPLC using a Phenomenex Luna 3 μm silica column (internal diameter 150 × 2.0 mm) under the following conditions: mobile phase A (chloroform: methanol: ammonium hydroxide, 89.5:10:0.5) and mobile phase B (chloroform: methanol: ammonium hydroxide: water, 55:39:0.5:5.5). Free FAs were quantitated using d31–16:0 (Sigma–Aldrich) and d8-20:4 (Cayman Chemicals) as internal standards.

4.6. Flow cytometry sorting of macrophages from callus tissues

Mice with femoral fractures from the indicated groups were euthanized, and the callus tissues were collected in MACS tissue storage solution (130-100-008, Miltenyi Biotec, Germany) at 4 °C. Then, the callus tissues around the TZ were carefully dissected and minced with tissue lysis buffer (25200-56 & A004174-0100, Biomarker Technologies, Beijing, China). After digestion for 1 h, the digested callus tissues were filtered through a 70 mm strainer. Tissue suspensions were centrifuged at 300 g for 5 min at 4 °C. Red blood cells were lysed in red blood cell lysis buffer (R1010, Solarbio, Beijing, China). For staining, cells were resuspended and incubated with the following antibodies (100 μl/1 × 10^6 cells) for 20–30 min at 4 °C in the dark: viability dye-ApCy7, anti-CD45-PerCP Cy™5.5, anti-CD11b-BV421, anti-F4/80-PE, and anti-MSR1-FITC. Afterward, the cells were washed and resuspended in 500 μl of cold PBS supplemented with 1% FBS before flow sorting using a FACSAria II SORP instrument (BD, USA). Finally, isolated callus macrophages ($CD45^+CD11b^+F4/80^+$) were collected in RPMI 1640 supplemented with 10% FBS and a 1% antibiotic mixture.

4.7. Statistical analyses

In all cases, data are presented as the means ± s.d. from at least three independent biological replicates. GraphPad Prism 7 (GraphPad Software, La Jolla, CA, USA), SPSS software version 25.0 (SPSS, Inc., Chicago, IL, USA) and ImageJ (NIH, USA) were used to conduct statistical analyses. Unpaired two-tailed Student's t-test was used for comparisons between two groups, and one-way analysis of variance was performed for multigroup comparisons. The chi-square test was used to examine the differences between the variables, and the Pearson correlation coefficient was calculated to detect the relationship between BMP7 production and ΔOCR of respiratory capacity or basal respiration.

Differences between groups were considered significant at a p value < 0.05.

Author contributions

S.J.Z., G.Y.Y., H.W.Z., J.C. and Z.Y.Z. were responsible for the concept and experimental design. Z.Y.Z., T.J., Z.F.H., B.C., J.G., X.Z. and H.L. performed the experiments, data analysis and statistical analysis. J. F., L.P.Y., S.H.J., Q.L., L.P.H., F.Q.K. and Q.C. provided technical and material support. S.J.Z and Z.Y.Z. were involved in drafting and revision of the manuscript. G.Y.Y., H.W.Z. and J.C. supervised this study. All authors discussed the results and commented on the manuscript.

Funding

This study was supported by grants from the National Natural Science Foundation of China [81902211, 82030069, 81772351, 8151001184 and 82102570], the Jiangsu Natural Science Foundation [BK20191061 and BK20191493], the Jiangsu Committee of Science and Technology-Social Development Plan [BE201755], the Young Scholars Fostering Fund of the First Affiliated Hospital of Nanjing Medical University [PY2021012] and the Postgraduate Research & Practice Innovation Program of Jiangsu Province [KYCX20_1385 and KYCX21_1608].

Declaration of competing interest

The authors have declared that no competing interest exists.

Acknowledgement

We are grateful to Hui Bai, Jing-Jing Ben, Xu-Dong Zhu, Xiao-Yu Li, Qing Yang and Ya-Qing Yang (Key Laboratory of Targeted Intervention of Cardiovascular Disease, Collaborative Innovation Center for Cardiovascular Disease Translational Medicine, Nanjing Medical University, Nanjing, China) for assistance with our experiments.

Appendix A. Supplementary data

Supplementary data to this article can be found online at https://doi.org/10.1016/j.redox.2022.102326.

References

[1] G.B. Reahl, L. Gerstenfeld, M. Kain, Epidemiology, clinical assessments, and current treatments of nonunions, Curr. Osteoporos. Rep. 18 (3) (2020) 157–168, https://doi.org/10.1007/s11914-020-00575-6.
[2] R.J. O'Keefe, Fibrinolysis as a target to enhance fracture healing, N. Engl. J. Med. 373 (18) (2015) 1776–1778, https://doi.org/10.1056/NEJMcibr1510090.
[3] C. Schlundt, T. El Khassawna, A. Serra, A. Dienelt, S. Wendler, H. Schell, et al., Macrophages in bone fracture healing: their essential role in endochondral ossification, Bone 106 (2018) 78–89, https://doi.org/10.1016/j.bone.2015.10.019.
[4] H. Kawahata, D. Sotobayashi, M. Aoki, H. Shimizu, H. Nakagami, T. Ogihara, et al., Continuous infusion of angiotensin II modulates hypertrophic differentiation and apoptosis of chondrocytes in cartilage formation in a fracture model mouse, Hypertens. Res. 38 (6) (2015) 382–393, https://doi.org/10.1038/hr.2015.18.
[5] P. Aghajanian, S. Mohan, The art of building bone: emerging role of chondrocyte-to-osteoblast transdifferentiation in endochondral ossification, Bone Res. 6 (2018) 19, https://doi.org/10.1038/s41413-018-0021-z.
[6] Z. Ding, M. Qiu, M.A. Alharbi, T. Huang, X. Pei, T.N. Milovanova, et al., FOXO1 expression in chondrocytes modulates cartilage production and removal in fracture healing, Bone 148 (2021) 115905, https://doi.org/10.1016/j.bone.2021.115905.
[7] M. Locati, G. Curtale, A. Mantovani, Diversity, mechanisms, and significance of macrophage plasticity, Annual Rev. Pathol. 15 (2020) 123–147, https://doi.org/10.1146/annurev-pathmechdis-012418-012718.
[8] S. Elmore, Apoptosis: a review of programmed cell death, Toxicol. Pathol. 35 (4) (2007) 495–516, https://doi.org/10.1080/01926230701320337.
[9] C.B. Medina, P. Mehrotra, S. Arandjelovic, J.S.A. Perry, Y. Guo, S. Morioka, et al., Metabolites released from apoptotic cells act as tissue messengers, Nature 580 (7801) (2020) 130–135, https://doi.org/10.1038/s41586-020-2121-3.
[10] A. Villalvilla, R. Gómez, R. Largo, G. Herrero-Beaumont, Lipid transport and metabolism in healthy and osteoarthritic cartilage, Int. J. Mol. Sci. 14 (10) (2013) 20793–20808, https://doi.org/10.3390/ijms141020793.
[11] J.L. Kelley, T.R. Ozment, C. Li, J.B. Schweitzer, D.L. Williams, Scavenger receptor-A (CD204): a two-edged sword in health and disease, Crit. Rev. Immunol. 34 (3) (2014) 241–261, https://doi.org/10.1615/critrevimmunol.2014010267.
[12] Y. He, S. Zhou, F. Deng, S. Zhao, W. Chen, D. Wang, et al., Clinical and transcriptional signatures of human CD204 reveal an applicable marker for the protumor phenotype of tumor-associated macrophages in breast cancer, Aging 11 (23) (2019) 10883–10901, https://doi.org/10.18632/aging.102490.
[13] M. Guo, A. Härtlova, M. Gierliński, A. Prescott, J. Castellvi, J.H. Losa, et al., Triggering MSR1 promotes JNK-mediated inflammation in IL-4-activated macrophages, EMBO J. 38 (11) (2019), https://doi.org/10.15252/embj.2018100299.
[14] S.J. Zhao, F.Q. Kong, J. Jie, Q. Li, H. Liu, A.D. Xu, et al., Macrophage MSR1 promotes BMSC osteogenic differentiation and M2-like polarization by activating PI3K/AKT/GSK3β/β-catenin pathway, Theranostics 10 (1) (2020) 17–35, https://doi.org/10.7150/thno.36930.
[15] C.S. Bahney, R.L. Zondervan, P. Allison, A. Theologis, J.W. Ashley, J. Ahn, et al., Cellular biology of fracture healing, J. Orthop. Res. 37 (1) (2019) 35–50, https://doi.org/10.1002/jor.24170.
[16] L. Claes, S. Recknagel, A. Ignatius, Fracture healing under healthy and inflammatory conditions, Nat. Rev. Rheumatol. 8 (3) (2012) 133–143, https://doi.org/10.1038/nrrheum.2012.1.
[17] M. Haffner-Luntzer, S. Foertsch, V. Fischer, K. Prystaz, M. Tschaffon, Y. Mödinger, et al., Chronic psychosocial stress compromises the immune response and endochondral ossification during bone fracture healing via β-AR signaling, Proc. Natl. Acad. Sci. U. S. A. 116 (17) (2019) 8615–8622, https://doi.org/10.1073/pnas.1819218116.
[18] A. Rigotti, Scavenger receptors and atherosclerosis, Biol. Res. 33 (2) (2000) 97–103, https://doi.org/10.4067/s0716-97602000000200009.
[19] I.Y. Benador, M. Veliova, M. Liesa, O.S. Shirihai, Mitochondria bound to lipid droplets: where mitochondrial dynamics regulate lipid storage and utilization, Cell Metabol. 29 (4) (2019) 827–835, https://doi.org/10.1016/j.cmet.2019.02.011.
[20] J. Van den Bossche, L.A. O'Neill, D. Menon, Macrophage immunometabolism: where are we (going)? Trends Immunol. 38 (6) (2017) 395–406, https://doi.org/10.1016/j.it.2017.03.001.
[21] A.Z. Mirza, Althagafi II, H. Shamshad, Role of PPAR receptor in different diseases and their ligands: physiological importance and clinical implications, Eur. J. Med. Chem. 166 (2019) 502–513, https://doi.org/10.1016/j.ejmech.2019.01.067.
[22] N. Bougarne, B. Weyers, S.J. Desmet, J. Deckers, D.W. Ray, B. Staels, et al., Molecular actions of PPARα in lipid metabolism and inflammation, Endocr. Rev. 39 (5) (2018) 760–802, https://doi.org/10.1210/er.2018-00064.
[23] T.J. Grevengoed, S.A. Martin, L. Katunga, D.E. Cooper, E.J. Anderson, R. C. Murphy, et al., Acyl-CoA synthetase 1 deficiency alters cardiolipin species and impairs mitochondrial function, J. Lipid Res. 56 (8) (2015) 1572–1582, https://doi.org/10.1194/jlr.M059717.
[24] A. Batista-Gonzalez, R. Vidal, A. Criollo, L.J. Carreño, New insights on the role of lipid metabolism in the metabolic reprogramming of macrophages, Front. Immunol. 10 (2019) 2993, https://doi.org/10.3389/fimmu.2019.02993.
[25] D.G. Ryan, L.A.J. O'Neill, Krebs cycle reborn in macrophage immunometabolism, Annu. Rev. Immunol. 38 (2020) 289–313, https://doi.org/10.1146/annurev-immunol-081619-104850.
[26] L.K. Billingham, N.S. Chandel, NAD-biosynthetic pathways regulate innate immunity, Nat. Immunol. 20 (4) (2019) 380–382, https://doi.org/10.1038/s41590-019-0353-x.
[27] S. Imai, L. Guarente, NAD+ and sirtuins in aging and disease, Trends Cell Biol. 24 (8) (2014) 464–471, https://doi.org/10.1016/j.tcb.2014.04.002.
[28] Q. Li, J.C. Cheng, Q. Jiang, W.Y. Lee, Role of sirtuins in bone biology: potential implications for novel therapeutic strategies for osteoporosis, Aging Cell 20 (2) (2021), e13301, https://doi.org/10.1111/acel.13301.
[29] Y. Chen, F. Zhou, H. Liu, J. Li, H. Che, J. Shen, et al., SIRT1, a promising regulator of bone homeostasis, Life Sci. 269 (2021) 119041, https://doi.org/10.1016/j.lfs.2021.119041.
[30] Y. Jing, Y. Zhou, F. Zhou, X. Wang, B. Tao, L. Sun, et al., SIRT2 deficiency prevents age-related bone loss in rats by inhibiting osteoclastogenesis, Cell. Mol. Biol. 65 (7) (2019) 66–71.
[31] J. Gao, Z. Feng, X. Wang, M. Zeng, J. Liu, S. Han, et al., SIRT3/SOD2 maintains osteoblast differentiation and bone formation by regulating mitochondrial stress, Cell Death Differ. 25 (2) (2018) 229–240, https://doi.org/10.1038/cdd.2017.144.
[32] M. Fukuda, T. Yoshizawa, M.F. Karim, S.U. Sobuz, W. Korogi, D. Kobayasi, et al., SIRT7 has a critical role in bone formation by regulating lysine acylation of SP7/Osterix, Nat. Commun. 9 (1) (2018) 2833, https://doi.org/10.1038/s41467-018-05187-4.
[33] C.N. Yang, S.K. Lin, S.H. Kok, H.W. Wang, Y.L. Lee, C.T. Shun, et al., The possible role of sirtuin 5 in the pathogenesis of apical periodontitis, Oral Dis. 27 (7) (2021) 1766–1774, https://doi.org/10.1111/odi.13723.
[34] Y.J. Moon, Z. Zhang, I.H. Bang, O.K. Kwon, S.J. Yoon, J.R. Kim, et al., Sirtuin 6 in preosteoclasts suppresses age- and estrogen deficiency-related bone loss by stabilizing estrogen receptor α, Cell Death Differ. 26 (11) (2019) 2358–2370, https://doi.org/10.1038/s41418-019-0306-9.
[35] T. Finkel, C.X. Deng, R. Mostoslavsky, Recent progress in the biology and physiology of sirtuins, Nature 460 (7255) (2009) 587–591, https://doi.org/10.1038/nature08197.
[36] M.A. Zaini, C. Müller, T.V. de Jong, T. Ackermann, G. Hartleben, G. Kortman, et al., A p300 and SIRT1 regulated acetylation switch of C/EBPα controls mitochondrial function, Cell Rep. 22 (2) (2018) 497–511, https://doi.org/10.1016/j.celrep.2017.12.061.

[37] R.H. Wang, X. Xu, H.S. Kim, Z. Xiao, C.X. Deng, SIRT1 deacetylates FOXA2 and is critical for Pdx1 transcription and β-cell formation, Int. J. Biol. Sci. 9 (9) (2013) 934–946, https://doi.org/10.7150/ijbs.7529.
[38] P. Simic, E.O. Williams, E.L. Bell, J.J. Gong, M. Bonkowski, L. Guarente, SIRT1 suppresses the epithelial-to-mesenchymal transition in cancer metastasis and organ fibrosis, Cell Rep. 3 (4) (2013) 1175–1186, https://doi.org/10.1016/j.celrep.2013.03.019.
[39] M.R. Kang, S.W. Lee, E. Um, H.T. Kang, E.S. Hwang, E.J. Kim, et al., Reciprocal roles of SIRT1 and SKIP in the regulation of RAR activity: implication in the retinoic acid-induced neuronal differentiation of P19 cells, Nucleic Acids Res. 38 (3) (2010) 822–831, https://doi.org/10.1093/nar/gkp1056.
[40] L. Du, X. Qian, Y. Li, X.Z. Li, L.L. He, L. Xu, et al., Sirt1 inhibits renal tubular cell epithelial-mesenchymal transition through YY1 deacetylation in diabetic nephropathy, Acta Pharmacol. Sin. 42 (2) (2021) 242–251, https://doi.org/10.1038/s41401-020-0450-2.
[41] L. Tiberi, J. van den Ameele, J. Dimidschstein, J. Piccirilli, D. Gall, A. Herpoel, et al., BCL6 controls neurogenesis through Sirt1-dependent epigenetic repression of selective Notch targets, Nat. Neurosci. 15 (12) (2012) 1627–1635, https://doi.org/10.1038/nn.3264.
[42] Z. Gao, J. Ye, Inhibition of transcriptional activity of c-JUN by SIRT1, Biochem. Biophys. Res. Commun. 376 (4) (2008) 793–796, https://doi.org/10.1016/j.bbrc.2008.09.079.
[43] N. Skrypek, K. Bruneel, C. Vandewalle, E. De Smedt, B. Soen, N. Loret, et al., ZEB2 stably represses RAB25 expression through epigenetic regulation by SIRT1 and DNMTs during epithelial-to-mesenchymal transition, Epigenet. Chromatin 11 (1) (2018) 70, https://doi.org/10.1186/s13072-018-0239-4.
[44] L. Qiang, H.V. Lin, J.Y. Kim-Muller, C.L. Welch, W. Gu, D. Accili, Proatherogenic abnormalities of lipid metabolism in SirT1 transgenic mice are mediated through Creb deacetylation, Cell Metabol. 14 (6) (2011) 758–767, https://doi.org/10.1016/j.cmet.2011.10.007.
[45] Q. Liu, H. Li, J. Wang, L. Zhong, X. Chen, R. Zhang, et al., Glucose restriction delays senescence and promotes proliferation of HUVECs via the AMPK/SIRT1-FOXA3-Beclin1 pathway, Exp. Gerontol. 139 (2020) 111053, https://doi.org/10.1016/j.exger.2020.111053.
[46] N. Stankovic-Valentin, S. Deltour, J. Seeler, S. Pinte, G. Vergoten, C. Guérardel, et al., An acetylation/deacetylation-SUMOylation switch through a phylogenetically conserved psiKXEP motif in the tumor suppressor HIC1 regulates transcriptional repression activity, Mol. Cell Biol. 27 (7) (2007) 2661–2675, https://doi.org/10.1128/mcb.01098-06.
[47] S. Kong, S.J. Kim, B. Sandal, S.M. Lee, B. Gao, D.D. Zhang, et al., The type III histone deacetylase Sirt1 protein suppresses p300-mediated histone H3 lysine 56 acetylation at Bclaf1 promoter to inhibit T cell activation, J. Biol. Chem. 286 (19) (2011) 16967–16975, https://doi.org/10.1074/jbc.M111.218206.
[48] N. Guida, G. Laudati, S. Anzilotti, A. Secondo, P. Montuori, G. Di Renzo, et al., Resveratrol via sirtuin-1 downregulates RE1-silencing transcription factor (REST) expression preventing PCB-95-induced neuronal cell death, Toxicol. Appl. Pharmacol. 288 (3) (2015) 387–398, https://doi.org/10.1016/j.taap.2015.08.010.
[49] J. Wan, J. Zhan, S. Li, J. Ma, W. Xu, C. Liu, et al., PCAF-primed EZH2 acetylation regulates its stability and promotes lung adenocarcinoma progression, Nucleic Acids Res. 43 (7) (2015) 3591–3604, https://doi.org/10.1093/nar/gkv238.
[50] E. Katsuyama, A. Suarez-Fueyo, S.J. Bradley, M. Mizui, A.V. Marin, L. Mulki, et al., The CD38/NAD/SIRTUIN1/EZH2 Axis mitigates cytotoxic CD8 T cell function and identifies patients with SLE prone to infections, Cell Rep. 30 (1) (2020) 112–123, https://doi.org/10.1016/j.celrep.2019.12.014, e4.
[51] C.S. Adams, I.M. Shapiro, The fate of the terminally differentiated chondrocyte: evidence for microenvironmental regulation of chondrocyte apoptosis, Crit. Rev. Oral Biol. Med. 13 (6) (2002) 465–473, https://doi.org/10.1177/154411130201300604.
[52] Y. Liu, R. Xu, H. Gu, E. Zhang, J. Qu, W. Cao, et al., Metabolic reprogramming in macrophage responses, Biomaker Res. 9 (1) (2021) 1, https://doi.org/10.1186/s40364-020-00251-y.
[53] S. Zhang, S. Weinberg, M. DeBerge, A. Gainullina, M. Schipma, J.M. Kinchen, et al., Efferocytosis fuels requirements of fatty acid oxidation and the electron transport chain to polarize macrophages for tissue repair, Cell Metabol. 29 (2) (2019) 443–456, https://doi.org/10.1016/j.cmet.2018.12.004, e5.
[54] R.C. Casarin, M.Z. Casati, S.P. Pimentel, F.R. Cirano, M. Algayer, P.R. Pires, et al., Resveratrol improves bone repair by modulation of bone morphogenetic proteins and osteopontin gene expression in rats, Int. J. Oral Maxillofac. Surg. 43 (7) (2014) 900–906, https://doi.org/10.1016/j.ijom.2014.01.009.
[55] L. Gan, Y. Yang, Q. Li, Y. Feng, T. Liu, W. Guo, Epigenetic regulation of cancer progression by EZH2: from biological insights to therapeutic potential, Biomaker Res. 6 (2018) 10, https://doi.org/10.1186/s40364-018-0122-2.
[56] S. Hemming, D. Cakouros, J. Codrington, K. Vandyke, A. Arthur, A. Zannettino, et al., EZH2 deletion in early mesenchyme compromises postnatal bone microarchitecture and structural integrity and accelerates remodeling, Faseb. J. 31 (3) (2017) 1011–1027, https://doi.org/10.1096/fj.201600748R.
[57] X. Wang, M. de Carvalho Ribeiro, A. Iracheta-Vellve, P. Lowe, A. Ambade, A. Satishchandran, et al., Macrophage-specific hypoxia-inducible factor-1α contributes to impaired autophagic flux in nonalcoholic steatohepatitis, Hepatology 69 (2) (2019) 545–563, https://doi.org/10.1002/hep.30215.
[58] J. Ji, D. Shu, M. Zheng, J. Wang, C. Luo, Y. Wang, et al., Microbial metabolite butyrate facilitates M2 macrophage polarization and function, Sci. Rep. 6 (2016) 24838, https://doi.org/10.1038/srep24838.
[59] S. Lucas, Y. Omata, J. Hofmann, M. Böttcher, A. Iljazovic, K. Sarter, et al., Short-chain fatty acids regulate systemic bone mass and protect from pathological bone loss, Nat. Commun. 9 (1) (2018) 55, https://doi.org/10.1038/s41467-017-02490-4.
[60] B. Luo, W. Gan, Z. Liu, Z. Shen, J. Wang, R. Shi, et al., Erythropoeitin signaling in macrophages promotes dying cell clearance and immune tolerance, Immunity 44 (2) (2016) 287–302, https://doi.org/10.1016/j.immuni.2016.01.002.
[61] S.J. Zhao, H. Liu, J. Chen, D.F. Qian, F.Q. Kong, J. Jie, et al., Macrophage GIT1 contributes to bone regeneration by regulating inflammatory responses in an ERK/NRF2-Dependent way, J. Bone Miner. Res. 35 (10) (2020) 2015–2031, https://doi.org/10.1002/jbmr.4099.
[62] H.J. Wright, J. Hou, B. Xu, M. Cortez, E.O. Potma, B.J. Tromberg, et al., CDCP1 drives triple-negative breast cancer metastasis through reduction of lipid-droplet abundance and stimulation of fatty acid oxidation, Proc. Natl. Acad. Sci. U. S. A. 114 (32) (2017), E6556-e65, https://doi.org/10.1073/pnas.1703791114.